TM185400

THESIS

TWO-WHEELED VEHICLE BALANCING USING CONTROL MOMENT GYROSCOPE

BUNTHENG CHHORN
ID. 02111850087002

ADVISOR
Dr. Eng Unggul Wasiwitono, ST., M.Eng.Sc.

MASTER PROGRAM
FIELD OF SYSTEMS AND CONTROL ENGINEERING
MECHANICAL ENGINEERING DEPARTMENT
FAKULTAS TEKNOLOGI INDUSTRI
INSTITUT TEKNOLOGI SEPULUH NOPEMBER
SURABAYA
2020

TM185400

THESIS

TWO-WHEELED VEHICLE BALANCING USING CONTROL MOMENT GYROSCOPE

BUNTHENG CHHORN
ID. 02111850087002

ADVISOR
Dr. Eng Unggul Wasiwitono, ST., M.Eng.Sc.

MASTER PROGRAM
FIELD OF SYSTEMS AND CONTROL ENGINEERING
MECHANICAL ENGINEERING DEPARTMENT
FAKULTAS TEKNOLOGI INDUSTRI
INSTITUT TEKNOLOGI SEPULUH NOPEMBER
SURABAYA
2020

TWO-WHEELED VEHICLE BALANCING USING CONTROL MOMENT GYROSCOPE

TUGAS AKHIR
Diajukan Untuk Memenuhi Salah Satu Syarat
Memperoleh Gelar Magister Teknik
Program Studi S-2 Departemen Teknik Mesin
Fakultas Teknologi Industri dan Rekayasa Sistem
Institut Teknologi Sepuluh Nopember

Oleh :
BUNTHENG CHHORN
NRP. 02111850087002

Tanggal Ujian: 03 Agustus 2020
Periode Wisuda: September 2020

Disetujui oleh Pembimbing Tugas Akhir :

1. **Dr. Eng Unggul Wasiwitono,ST., M.Eng.Sc**
   NIP. 197805102001121001
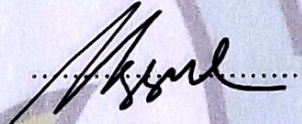
Penguji:

1. **Bambang Pramujati, S.T., M.Sc., Ph.D**
   NIP. 196912031994031001

2. **Prof. Ir. I Nyoman Sutantra, M.Sc., Ph.D**
   NIP. 195106051978031002

3. **Dr. Latifah Nurahmi, S.T., M.Sc**
   NIP. 1986201712037
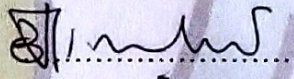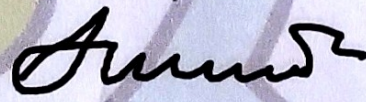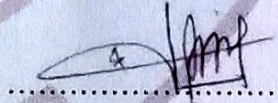
Kepala Departemen Teknik Mesin
FAKULTAS TEKNOLOGI INDUSTRI DAN REKAYASA SISTEM

Dr. Ir. Atok Setiyawan, M.Eng.Sc
NIP. 196604021985031003

This page is blank

TWO-WHEELED VEHICLE BALANCING USING CONTROL MOMENT GYROSCOPE

Student Name   : Buntheng Chhorn
NRP   : 02111850087002
Advisor   : Dr. Eng Unggul Wasiwitono, ST., M.Eng.Sc.

ABSTRACT

Two-wheeled vehicles have many advantages over other concepts such as smaller size, more efficient, and more maneuverable. These advantages came at the lack of stability and safety. To improve the stability and safety of a two-wheeled vehicle, the Control Moment Gyroscopic Stabilization is considered. The control problem of stabilizing an inherently unstable body such as the inverted pendulum is a classical control theory problem. The idea of using the gyroscope effect for stabilizing is part of a much broader effort to implement with the inverted pendulum. This phenomenon is known as gyroscopic precession. As the vehicle leans from its upright position, we expect to generate sufficient gyroscopic reaction moment to bring the vehicle back and stabilize it.

The research aims to develop and validate the system of gyroscopic stabilization to be implemented into a two-wheeled vehicle. The mathematical model by using the Lagrange equation is derived to descript the dynamic model of the system. We linearize the dynamics around an equilibrium, and then study the stability of the model. The feedback controller is applied to keep the system at upright position. In this study, we designed the cascade PID and the LQR controller. The proposed control technique is developed to reduce the roll effect the system. To validate the concept, a nonlinear modeling is developed using Simcape Multibody.

The control strategy is proposed to stabilize the two-wheeled vehicle at the upright position. The performance comparison between the cascade PID and modern control Linear Quadratic Regulator (LQR) schemes for a two-wheeled vehicle is investigated. In the comparison of cascade PID controller, the response

in case 6 takes fastest time to bring the vehicle to balancing position in 0.75s. However, the cascade PID controller cannot bring the shaft motor close to zero position after stabilizing the vehicle then the gyro would not be efficient of producing its maximum precession torque for the next disturbance introduced into the system which could possibly not be enough to stabilize the vehicle. The LQR produced a better response compared to cascade PID control strategies. The weighting in case 2 has good performance with fast response. Nonlinear simulation showed that each weighting can bring shaft motor close to zero position with range less than ±5 degree. To determine the ability of disturbance rejection, the simulation of the LQR controller succeeds to deal with the disturbances and it ensures stabilized in its upright position.

KESEIMBANGAN KENDARAAN DUA WHEELED MENGGUNAKAN GYROSCOPE KONTROL MOMEN

Nama   : Buntheng Chhorn
NRP   : 02111850087002
Dosen Pembimbing : Dr. Eng Unggul Wasiwitono, ST., M.Eng.Sc.

ABSTRAK

Kendaraan roda dua memiliki banyak keunggulan dibandingkan dengan konsep lain seperti ukurannya yang lebih kecil, lebih efisien, dan lebih bermanuver. Keuntungan ini datang dari kurangnya stabilitas dan keamanan. Untuk meningkatkan stabilitas dan keselamatan kendaraan roda dua, Stabilisasi Giroskop Momen Kontrol dipertimbangkan. Masalah kontrol menstabilkan benda yang secara inheren tidak stabil seperti pendulum terbalik adalah masalah teori kontrol klasik. Gagasan menggunakan efek giroskop untuk menstabilkan merupakan bagian dari upaya yang lebih luas untuk diterapkan dengan pendulum terbalik. Fenomena ini dikenal sebagai presesi giroskopik. Saat kendaraan bersandar dari posisi tegaknya, kami berharap dapat menghasilkan momen reaksi giroskopik yang cukup untuk mengembalikan kendaraan dan menstabilkannya.

Penelitian ini bertujuan untuk mengembangkan dan memvalidasi sistem stabilisasi giroskopik untuk diimplementasikan pada kendaraan roda dua. Model matematika dengan menggunakan persamaan Lagrange diturunkan untuk mendeskripsikan model dinamik sistem. Kami meluruskan dinamika di sekitar ekuilibrium, dan kemudian mempelajari stabilitas model. Pengontrol umpan balik diterapkan untuk menjaga sistem pada posisi tegak. Dalam studi ini, dirancang cascade PID dan pengontrol LQR. Teknik kontrol yang diusulkan dikembangkan untuk mengurangi efek roll sistem. Untuk memvalidasi konsep tersebut, dikembangkan pemodelan nonlinier menggunakan Simcape Multibody.

Strategi pengendalian diusulkan untuk menstabilkan kendaraan roda dua pada posisi tegak. Perbandingan kinerja antara cascade PID dan skema kontrol modern Linear Quadratic Regulator (LQR) untuk kendaraan roda dua diselidiki.

Dalam perbandingan kontroler PID bertingkat, respon pada kasus 6 membutuhkan waktu tercepat untuk membawa kendaraan ke posisi balancing dalam 0,75 detik. Namun, kontroler PID bertingkat tidak dapat membawa motor poros mendekati posisi nol setelah menstabilkan kendaraan, maka giro tidak akan efisien dalam menghasilkan torsi presesi maksimumnya untuk gangguan berikutnya yang dimasukkan ke dalam sistem yang mungkin tidak cukup untuk menstabilkan kendaraan. . LQR menghasilkan respons yang lebih baik dibandingkan dengan strategi kontrol PID berjenjang. Pembobotan pada case 2 memiliki kinerja yang baik dengan respon yang cepat. Simulasi nonlinier menunjukkan bahwa setiap pembobotan dapat membawa motor poros mendekati posisi nol dengan jarak kurang dari ± 5 derajat. Untuk mengetahui kemampuan penolakan gangguan, simulasi pengontrol LQR berhasil mengatasi gangguan dan memastikan stabil pada posisi tegak.

Kata kunci: Giroskop momen kontrol (CMG), Kontrol umpan balik, Stabilisasi Giroskopis, Sistem Tidak Stabil

ACKNOWLEDGEMENT

First and foremost, I would like to express my deep gratitude to my beloved **Parents** who inspire, touch and illuminate me through their presence, especially for their magnificent support, care, and love. It was under their watchful eyes that I gained so much drive and ability to tackle challenges head-on.

I gratefully acknowledge to **The Kemitraan Negara Berkembang (KNB) Scholarship**, a financial assistance offered by the **Indonesian Government** for international students to purse their master degree in Indonesia Universities, for the support the financial. It has been a memorable journey for my academic life during my unforgettable stay in Indonesia.

I would like to express our deep gratitude to my supervisor **Pak Unggul Wasiwitono**, who plays a crucial role during my researching. It is a great pleasure in thanking him for the patience he has shown in listening to all of my problems. With his immense support, guidance and kind attention, I can complete my report successfully.

I gratefully acknowledge to **IO volunteers and IO staffs** for their help and support all problems I met in Indonesia. Then, they spent their times to look after and make facility for all international students.

I truthfully thank you all!

TABLE OF CONTENT

This page is blank

LIST OF FIGURES

This page is blank

LIST OF TABLES

This page is blank

CHAPTER 1

INTRODUCTION

1.1. Background

The gyroscopic has been played an important role in many applications over a wide range of technical fields. Gyroscope is a device used for measuring or maintaining orientation and angular velocity. It is a spinning wheel in the spin axis. The idea using gyroscope movement is significant for applications in different fields of physics (e.g. Larmor precession in atomism) and astronomy (lunisolar precession of Earth), in technology (e.g. gyroscopic effect in transportation), in military (stabilization of missiles and bullets) and also in sport (flight disk), in energetics (kinetic energy accumulation by turbines, mechanical batteries). In [1], the implementation of gyroscopes can be divided into several groups: stabilizers, energy storage, gyrocompass, attitude and heading indicator, Pendulous Integrating Gyroscopic Accelerometer (PIGA), gyrostat, Control moment gyroscope (CMG), and MEMS Gyroscope. As mention above, they were known as two applications: passive (sensor) and actuator stabilization of the unstable dynamic system. Sensor applications such as navigation systems and passive stabilization systems used in ships while the gyroscope can also be used as an actuator by utilizing the precession phenomenon.

The control moment gyro (CMG) is one of the angular momentum exchange devices which is the application of this research that can produce large output torque on the body. It consists of the motor-driven rotor and gimbal. The spin axis of the flywheel can vary about a perpendicular axis to its spin axis (the gimbal axis). Complex dynamic derivations are used to find a relationship between the torque input to the gimbal axis and a desired output torque on the body. The rate of change of angular momentum between the CMG and the body is dependent on the gimbal velocity.

Figure 1.1 The Shilovsky's Gyrocar
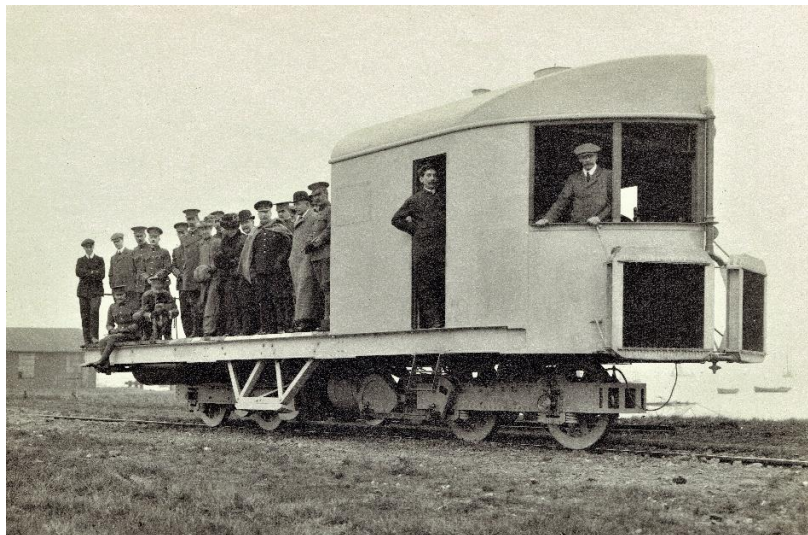
Figure 1.2 Brennan`s Monorail

CMG stabilization has been implemented since the 20th century, but the achievement was very restricted because of the high cost of motors, limited electric motor technology and lacking sensor feedback at the time. Perhaps the first notable implementation of gyroscopic stabilization is attached with two particular names; Louis Brennan [2] and Pyotr Shilovsky [3][4],[5], who build large-scale prototypes. The most famous vehicles are the Schilovsky Gyro car (Figure 1.1) in 1912 from Russia and Brennan`s Monorail (Figure 1.2) in 1962 from the USA.

1.2.   Research problem

Based on the above background, several problems can be formulated as follows:

- What is the relationship between the CMG dimension with the precession torque?
- How is the performance of feedback control for CMG?
- How to balance a two-wheeled vehicle using the phenomena of gyroscope?

1.3.   Research objectives

The purposes of this research are formulated as the following:

- Using Lagrange equation to describe dynamic model of the gyroscopic two-wheeled vehicle
- Design full state-feedback control to observe the performance of the gimbal stabilize the vehicle
- Compare the performance of PID and LQR controller

1.4.   Scope of research

The scope of this research is descript as following:

- Two active flywheels validated stabilizing only at the roll angle of the vehicle
- The balancing vehicle used is the gyroscopic control moment
- The designed controller of the gyroscope stabilization using the PID and LQR controller
- Both flywheel spin at the same constant velocity
- Modeling of the controller using Matlab/SIMULINK

This page is blank

CHAPTER 2

LITERATURE REVIEW

This section provides previous research and basic theory about the current technology available to construct gyroscope inverted pendulum. It also highlights various methods used that similar with this topic.

2.1 Previous Research

The two-wheeled Self-balancing vehicle, the idea based on the inverted pendulum model, has been being an essential and interesting project in the fields of robotics and control engineering. Over the last decade, the design and implementation of the self-balancing vehicle have been done and more work has already been done due to its natural unstable and nonlinearity dynamic system. In theory, there are several ways to stabilize a two-wheeled vehicle; but three methods have been proved to date. The most common method of stabilization is dynamic stabilization where the bicycle is actively steered to induce leans that oppose the bicycle's instabilities while moving forward at constant velocity [6]–[8]. The second method is moving the center of mass [9], [10]. Another one is using the gyroscope effect based on Control Moment Gyroscopic (CMG) stabilization (see in ref. [11]–[13]), which is the area of this research. In [13], the advantage of such a system is that it is efficiently producing a large amount of torque and has no ground reaction forces, while the disadvantage is that such system consumes more energy and is heavier. Today much progress has been made in electric motor technology as compared to a near-century ago. Currently, a recent start-up company based out of San-Francisco, CA, called Lit Motors, is using a set of 2 counter-rotating single-axis gimbal gyro's to stabilize and autonomously balance an enclosed motorcycle [14]. This completed electric vehicle is shown in Figure 2.1, has proven through prototype success the capability to stabilize and self-balance a vehicle that can transport up to two people.
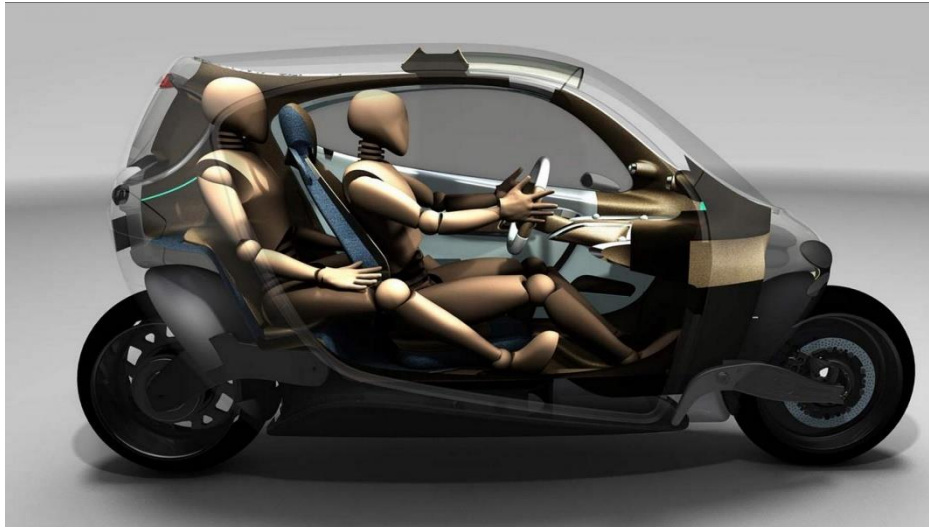
Figure 2.1 Lit Motor's self-balancing prototype

In applications of stabilizing the single-track vehicle using gyroscopes, Stephen and Anouck [12] derive the mathematic model using Lagrangian mechanics both single gyro and double gyro system. For the double gyro system, each of the two gyros and cages will have mass properties that are half those of the corresponding single gyro components. For simplicity, they assume that the center mass of the gyros and cages are collocated, each gyro spin opposite direction and the precession axes are the same. And then they linearize the dynamics about a set of equilibrium points and develop a linearized model. The full nonlinear dynamics were simulated, along with the linear feedback controller designed using Matlab. The stability conditions are dependent on turn rate and direction for the single gyro case, but not for the double gyro case. The full nonlinear dynamics were simulated, along with the linear feedback controller. The initial conditions for the vehicle's roll angle ϕ and gimbal's angle α are $\phi = 10\ deg$ and $\alpha = 25\ deg$. Two of controller gain are chosen to meet the stability condition. In Figure 2.2 shown the behavior of the gyro and cart angles for the different turn rates. With the same two values of turn rate, the double gyroscope system is stable for both cases. For the experiment a small-scaled model, the stability conditions are dependent on turn rate and direction for the single gyro case, but not for the double gyro case. This is also verified by simulation.
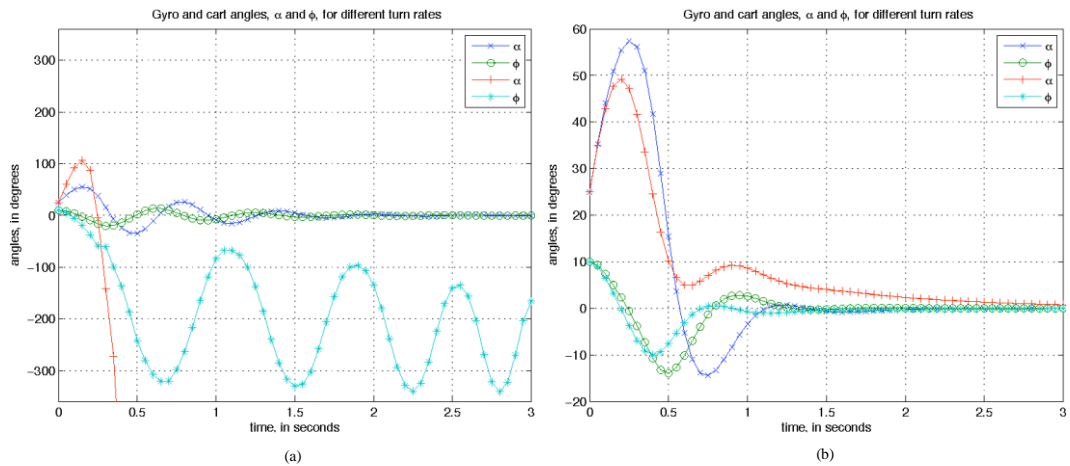
Figure 2.2 The Simulation: (a) Single Gyroscope (b) Double Gyroscope

In ref. [11], Chu and Chen proposed the design of an active stabilizing system (ASAS) for a single-track vehicle. The mathematical model for the inverted pendulum is derived using Lagrange's equation and then is verified by comparing the closed loop response with a model which is constructed using the commercial software ADAMS. To control the flywheel's gimbals for generating stabilizing torque, a model predictive control algorithm is used to synthesize the controllers. The prediction model for MPC is obtained by linearizing the nonlinear inverted pendulum. They evaluated the performance the control strategies of MPC in three cases. There are straight running and disturbance rejection, circular motion, and path following. The operating point of the system is the upright position and the gimbal angles are zero. In Figure 2.3, the design of the gyroscopic inverted pendulum contains two spinning flywheels attached to gimbal frames, four electric motors, and bevel gears. Both flywheels are rotating at a constant speed of 4000 rpm in the opposite direction. The results for the real-time implementation in this study demonstrate the feasibility of embedding the proposed controllers in common hardware.
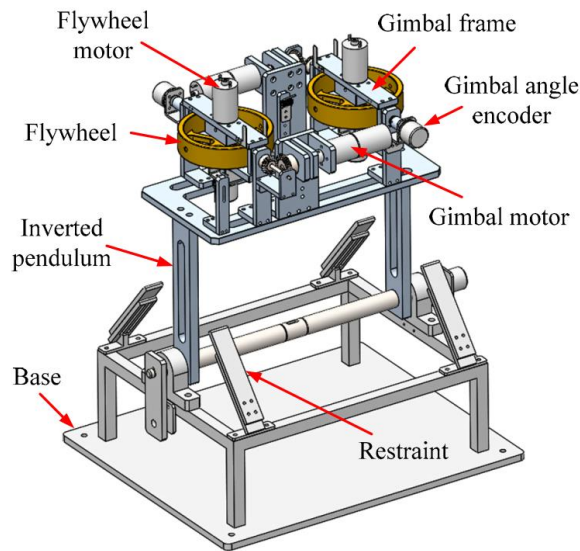
Figure 2.3 physical model of gyroscopic inverted pendulum

Hsieh, Ming-Hung, et al [15] designed a riderless bicycle with a gyroscopic balancer by using fuzzy sliding mode control (FSMC). In order to perform a simulation, they derived the bicycle dynamics model with the gyroscopic balancer according to the bicycle system. The bicycle system is considered as an inverted pendulum system with two independent masses (the mass center of the bicycle and the mass center of the gyroscopic balancer). To verify the control stability of the bicycle with the gyroscopic balancer controlled by FSMC, they conducted the simulation run in Matlab environment. In Figure 2.4 shown the balancing the unmoving bicycle hit by impact disturbances. The maximum lean angles of the bicycle disturbed by Gaussian noise and impact disturbances are approximately 4.0^o and 5.8^o, respectively, and the bicycle can still be balanced. The control voltage increases rapidly at 10th and 15th seconds to prevent the bicycle from falling down under impact disturbances. For the experiment, the unmoving vehicle can be still stabilized even interfered by disturbances.
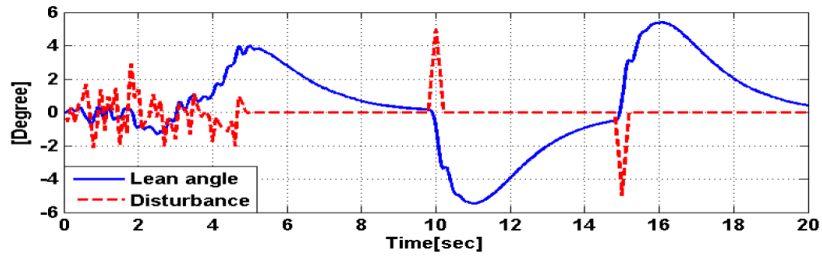
(a) Lean angle θ of the bicycle and disturbance.
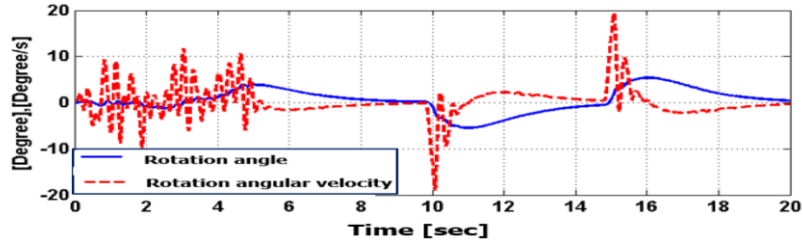
(b) Rotation angle φ and angular velocity of the flywheel
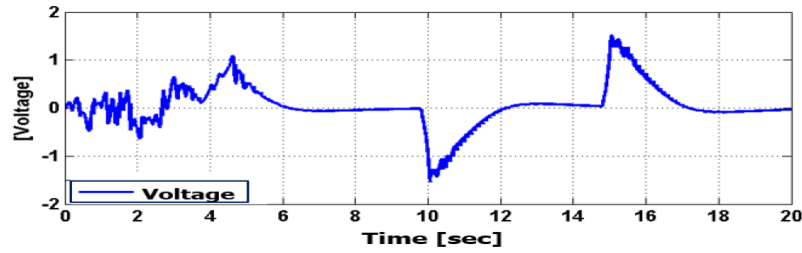
(c) Control input voltage U_f of the flywheel rotation motor

Figure 2.4 Unmoving bicycle with the balancer under disturbances

2.2   Basic Theory

2.2.1   Control Moment Gyroscope (CMG)

Control moment gyroscope (CMG) was known as a gyroscopic stabilizer is a good choice as the short time response and the system can be stable even when the single-track vehicles are stationary. CMG consists of a spinning rotor with large constant angular momentum although angular momentum vector direction would change with respect to single-track vehicles by rotating the spinning rotor. The spinning rotor is attached on a gimbal, and applying torque to the gimbal results in a precessional, gyroscopic reaction torque orthogonal to both the rotor spin and gimbal axes. The CMG is a torque amplification device because small gimbal torque input produces large control torque on the bicycle.

According to Newton's 1st law of motion, an object in motion will stay in motion unless acted on by an external force. This statement holds true for rotating objects as well. Therefore, a spinning flywheel (constant spin rate) with no applied

external forces or torques will continue to spin about its spin axis, in its current orientation, with no other rotational or translational motion relative to a stationary frame of reference. However, a spinning flywheel with a total of external forces or torques (about an axis other than its spin axis) not equal to zero exhibits an interesting phenomenon called precession [16]. To observe the precession effect caused by a rate of change of angular momentum, the flywheel must rotate about an axis perpendicular to its spin axis.
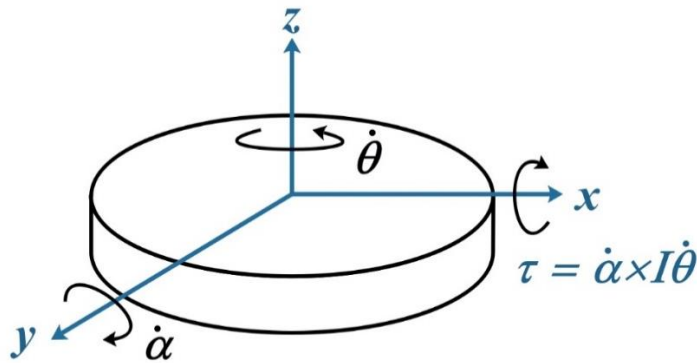
Figure 2.5 Gyrospoce Phenomena

In order to utilize this phenomenon for stabilization, the flywheel precession axis is supported to the frame such that the precession torque is transferred to the vehicle. In Figure 2.5, when there is an instability about the spin axis the spinning flywheel is turned or gimbaled. This results in a torque perpendicular to the gimbal and spin axis which can move the system back into a stable position.

In Figure 2.5, the flywheel or rotor is spinning around the z-axis with a spinning velocity $\dot{\theta}$. According to Newton's second law, the angular momentum created by the spinning gyroscope is given by:

$$T = I\dot{\theta} \tag{2.2.1}$$

Where I is the moment of inertia of the gyroscopic flywheel around the z-axis. I is derived as

$$I = \frac{1}{2}mR^2 \tag{2.2.2}$$

Where m is mass of the flywheel, and R is its radius. From Newton's third law we know that every action has its reaction. From Figure 2.5, gimbal rotates

10

around y-axis or precession angle at an angular velocity $\dot{\alpha}$ with specific torque, and therefore the gyroscope tries to resist the applied torque. As a result, it produces gyro torque along x-axis that can represent as

$$\vec{\tau} = \vec{T} \times \dot{\alpha} \qquad (2.2.3)$$

The stable torque produced by the control moment gyroscope can be expressed by (2.2.4) When the gimbal rotates 90°, there is no stable torque respect to the roll-axis. To efficiently stabilize roll-axis gimbal should have action within some small precession boundaries.

$$\tau_{stable} = \frac{1}{2} mR^2 \dot{\theta} \frac{d\alpha}{dt} \cos \alpha \qquad (2.2.4)$$

2.2.2   Lagrange Equation

Lagrangian equation, well-known equation to deal with mechanical problems in physics, used to analyze equations of motion based on energy. Lagrangian mechanics related to the dynamics of behavior, when Newton's formulation of classical mechanics was not much difficult. Lagrange's equations are also used in optimization problems of dynamic systems. In mechanics, Lagrange's equations of the second kind are used much more than the first kind. The Lagrange equation combines the kinetic energy denoted by (T) and the potential energy denoted by (V). The relationship between both energies can be written in equation (2.2.5).

$$L = T - V \qquad (2.2.5)$$

2.2.3   State Space

When systems become more complex, differential equations or transfer functions become inconvenient. It became true if the system has multiple inputs and outputs. In control engineering, a state-space is a mathematical model of a physical system as a set of input, output and state variables related difference equations. The state-space model of a system replaces an nth order differential equation with a single first-order matrix differential equation. The state-space of a system is given by two equations:

11

$$\dot{x} = Ax + Bu$$
$$y = Cx + Du$$

$$(2.2.6)$$

Where $\dot{x}$ is derivative of the state vector, x is the state vector, u is the input or control vector, A is state matrix contains the constant elements, B is input matrix contain constant element, C is output matrix, and D is the direct transition matrix, y is the output. The block diagram of the state space model is shown in Figure 2.6 in the form of blocks.
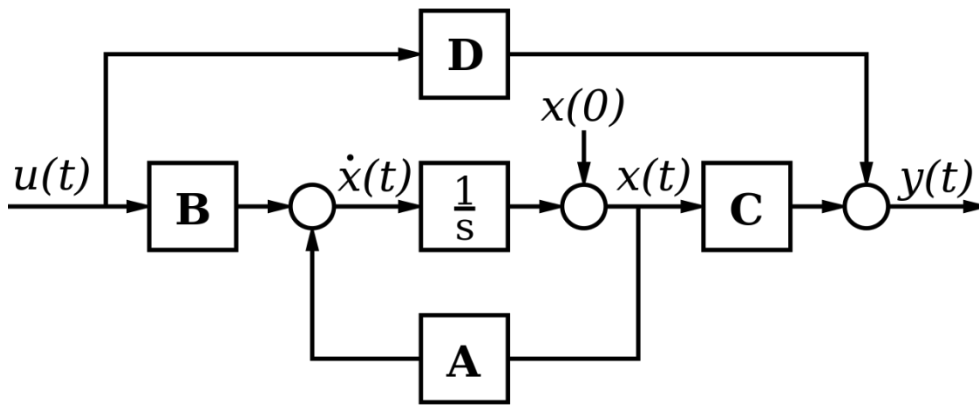
Figure 2.6 Block diagram of State Space

2.2.4 System Characteristics

In this section divided into three main parts. The first part contains important definitions of stability and necessary and sufficient conditions for stability. In the second part controllability of dynamical control system is described and, using the controllability matrix, necessary and sufficient conditions for controllability are presented. The third part is offered to a study of observability. In this part necessary and sufficient observability conditions are formulated using the observability matrix. Stability, controllability, and observability play an essential role in the development of modern mathematical control theory. There are notable associations between stability, controllability, and observability of linear control systems.

2.2.4.1 Controllability

For linear systems, there is a simple controllability criterion known as Kalman's controllability rank condition [17]. A linear system is a system defined by

$$\begin{cases} \dot{x} = X(x,u) = Ax + Bu \\ x \in \mathbb{R}^n, \mathbf{u} \in \mathbf{U} \subset \mathbb{R}^m \end{cases} \qquad (2.2.7)$$

where A and B are respectively $n \times n$ and $n \times m$ matrices. The model is controllability when the control set is $U = \mathbb{R}^m$ (there are no restrictions on the size of controls.). According to equation (2.2.7) is controllable, reachable from any point $x_0 \in \mathbb{R}^n$, reachable accessible from the origin $x_0 = 0$. The reachable set from the origin $A(0)$ is a linear subspace of $\mathbb{R}^n$. It is the image of the linear map:

$$\mathbb{R}^{m+n} \to \mathbb{R}^n$$

$$(\mathbf{u}_1,...,\mathbf{u}_n) \mapsto (\mathbf{B},\mathbf{AB},\mathbf{A}^2\mathbf{B},...,\mathbf{A}^{n-1}\mathbf{B}) \begin{pmatrix} u_1 \\ \vdots \\ u_n \end{pmatrix} = \sum_{i=1}^{n} A^{i-1} B u_i$$

The $n \times m$ block matrix $R(A,B) = (B, AB, A^2 B,\ldots, A^{n-1}B)$ whose columns are the columns of $B, AB, A^2 B,\ldots, A^{n-1}B$ is called the Kalman controllability matrix. The controllability of the linear system (2.2.7) is related to the rank of this matrix as follows

$$R(A,B) = (B, AB, A^2 B,\ldots, A^{n-1}B)$$

is of rank n (the dimension of the state space).

2.2.4.2 Stability

In [18], it is well known that the controllability concept for dynamical system (2.2.6) is strongly related to its stability by the linear static state feedback of the following form

$$u(t) = Kx(t) + v(t)$$

where $v(t) \in R^m$ is a new control, K is $m \times n$ dimensional constant state feedback matrix.

Introducing the linear static state feedback given by equality, we directly obtain the linear differential state equation for the feedback linear dynamical system of the following form

$$x'(t) = (A + BK)x(t) + Bv(t)$$

which is characterized by the pair of constant matrices $(A + BK, B)$. The dynamical system (2.2.6) is said to be stabilizable if there exists a constant static state feedback matrix K such that the spectrum of the matrix (A+BK) entirely lies in the left-hand side of the complex plane.

2.2.4.3 Observability

In [17], the observability properties of linear systems are defined as

$$\begin{cases} \dot{x}(t) = Ax(t) + Bu(t), \\ \qquad y(t) = Cx(t), \\ x(t) \in \mathbb{R}^n, u(t) \in U \subset \mathbb{R}^m, y(t) \in \mathbb{R}^q, \\ A, B, and\ C\ are\ respectively\ n \times n, n \times p\ and\ m \times n\ \dim ention \end{cases} \qquad (2.2.8)$$

We remark that this condition is independent of the input. So the linear system (2.2.8) is uniformly input observable if and only if it is observable if and only if the matrix:

$$O_{(C,A)} = \begin{pmatrix} C \\ CA \\ CA^2 \\ \vdots \\ CA^{n-1} \end{pmatrix}$$

is of rank n. In this case we say that the system (2.2.8), or the pair (C, A), satisfies the Kalman rank condition for observability.

2.2.5 Feedback Control System

There are two main types of feedback control systems: negative feedback and positive feedback. In a positive feedback control system, the setpoint and output values are added. In a negative feedback control the setpoint and output values are subtracted. Negative feedback systems are more stable than positive feedback systems. Negative feedback also makes systems more immune to random variations in component values and inputs.

2.2.5.1 PID Controller

The Proportional Integral Derivative (PID) control function shown in.(2.2.9) is the most popular choice in industry.

$$u = K_P e + K_I \int e\,dt + K_D \left(\frac{de}{dt} \right) \tag{2.2.9}$$

where u is the input signal to the plant model, the error signal e defined as $e(t) = r(t) - y(t)$, $r(t)$ is the reference input signal, and there are three separate gain constants for the three terms. The result is a control variable value. PID block diagram is shown in Figure 2.7.
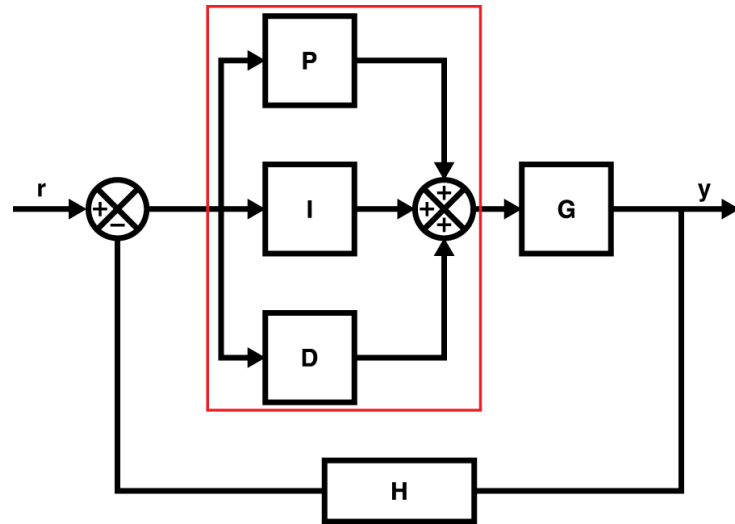
Figure 2.7. Block diagram of PID controller

2.2.5.2 LQR Controller

The Linear Quadratic Regulator (LQR) is a well-known method that provides optimally controlled feedback gains to enable the closed-loop stable and high-performance design of systems. The principle of using this LQR method is to obtain an optimal control signal from the state feedback. For the derivation of the linear quadratic regulator consider a linear system state-space representation in equation (2.2.6). The feedback gain is a matrix K obtained by solving the Riccati equation as shown in (2.2.10). Solving the Riccati equation is done in software because it is quite complicated if solved manually.

$$\frac{dP}{dt} = A^T P + PA + Q - PBR^{-1}B^T P = 0 \tag{2.2.10}$$

Where A and B are obtained from state-space model. Q and R values are weighted whose value is tested using trial and error. The weight given to the ith element of the matrix Q is a measurement of the control effort to control the related state. The bigger element, the bigger control effort used for that state. In [19], the matrix R is a $p \times p$, real, symmetric, positive-definite matrix. The gain value K can be solved by the equation:

$$K(t) = R^{-1}B^T P \qquad (2.2.11)$$

The performance index is used to minimizing both the control effort and the states can be given as:

$$J = \frac{1}{2}\int_0^\infty (\mathbf{x}^T Q\mathbf{x} + \mathbf{u}^T R\mathbf{u})\,dt \qquad (2.2.12)$$

Block diagram of the optimal control system with state feedback values can be seen in Figure 2.8.
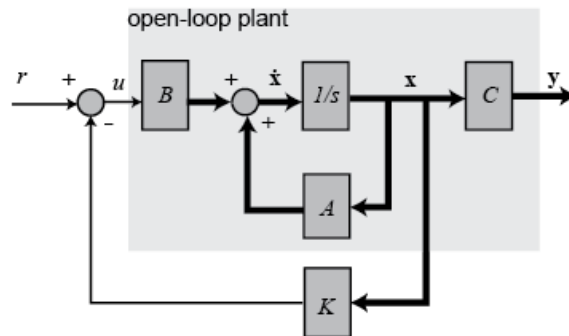
Figure 2.8 Block Diagram of LQR controller

This page is blank

CHAPTER 3

METHODOLOGY

This chapter, the through process will describe in the flow chart. Then the concepts and the components of the gyroscopic two-wheeled vehicle will illustrate. Later, the vehicle's equations of motion are derived based on Lagrangian mechanics. In addition, the linearized model together with the DC motors dynamics are merged into one unified state space model.

3.1   Research flow chart

The procedure of each part for this project are illustrated in Figure 3.1 Flowchart of the processFigure 3.1. The concept of design PID and LQR controller showed in Figure 3.2 and Figure 3.3, respectively.
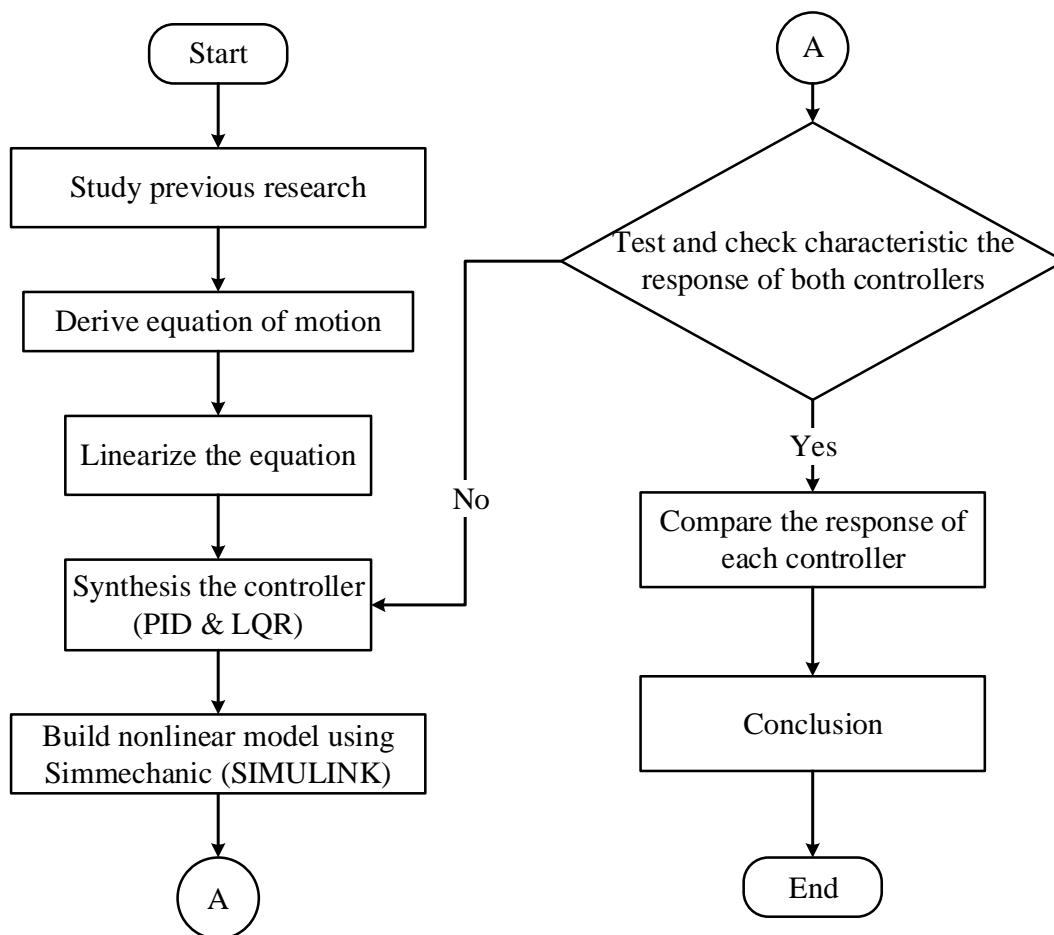
Figure 3.1 Flowchart of the process
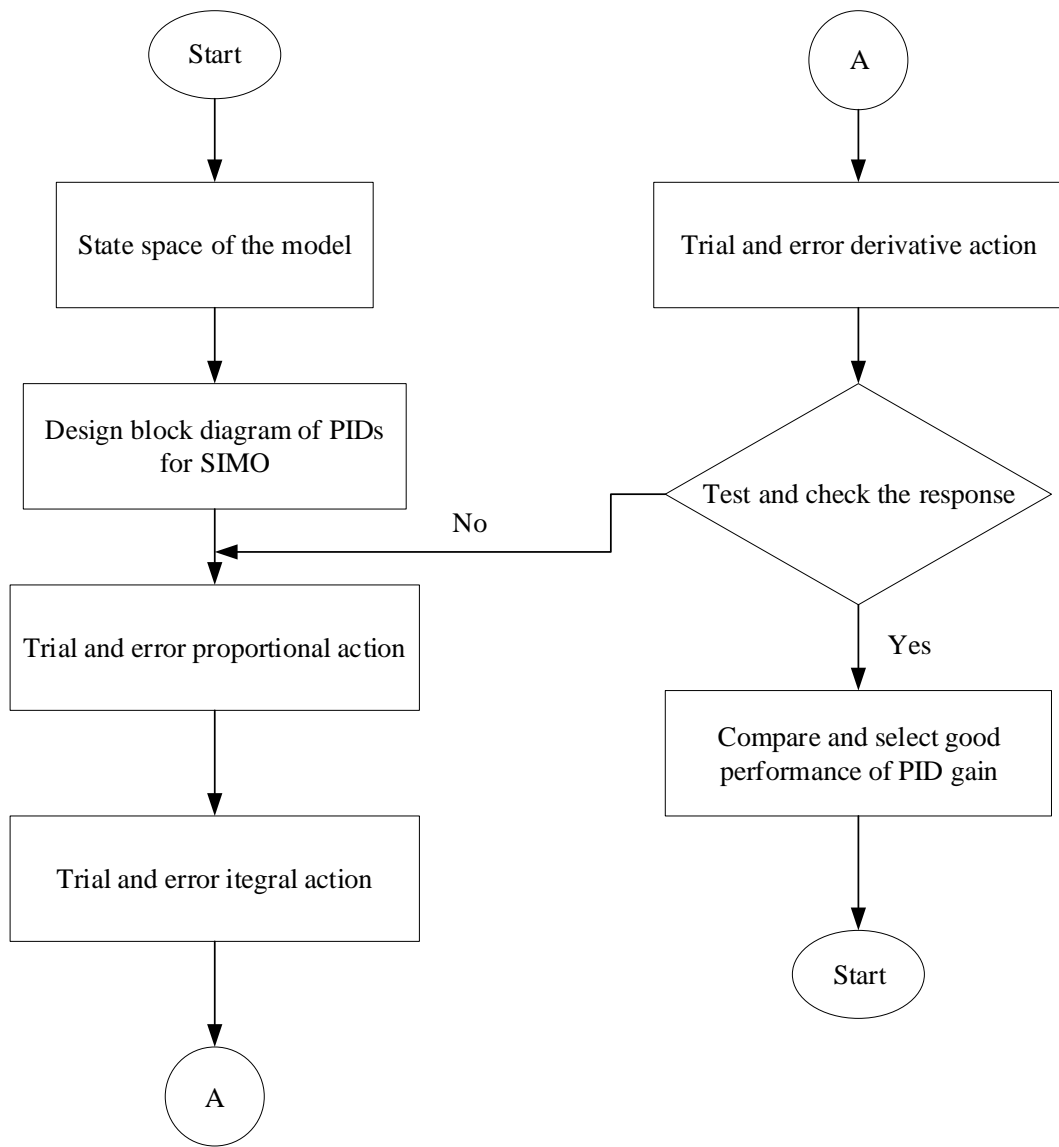
Figure 3.2. The procedure of design PID controller
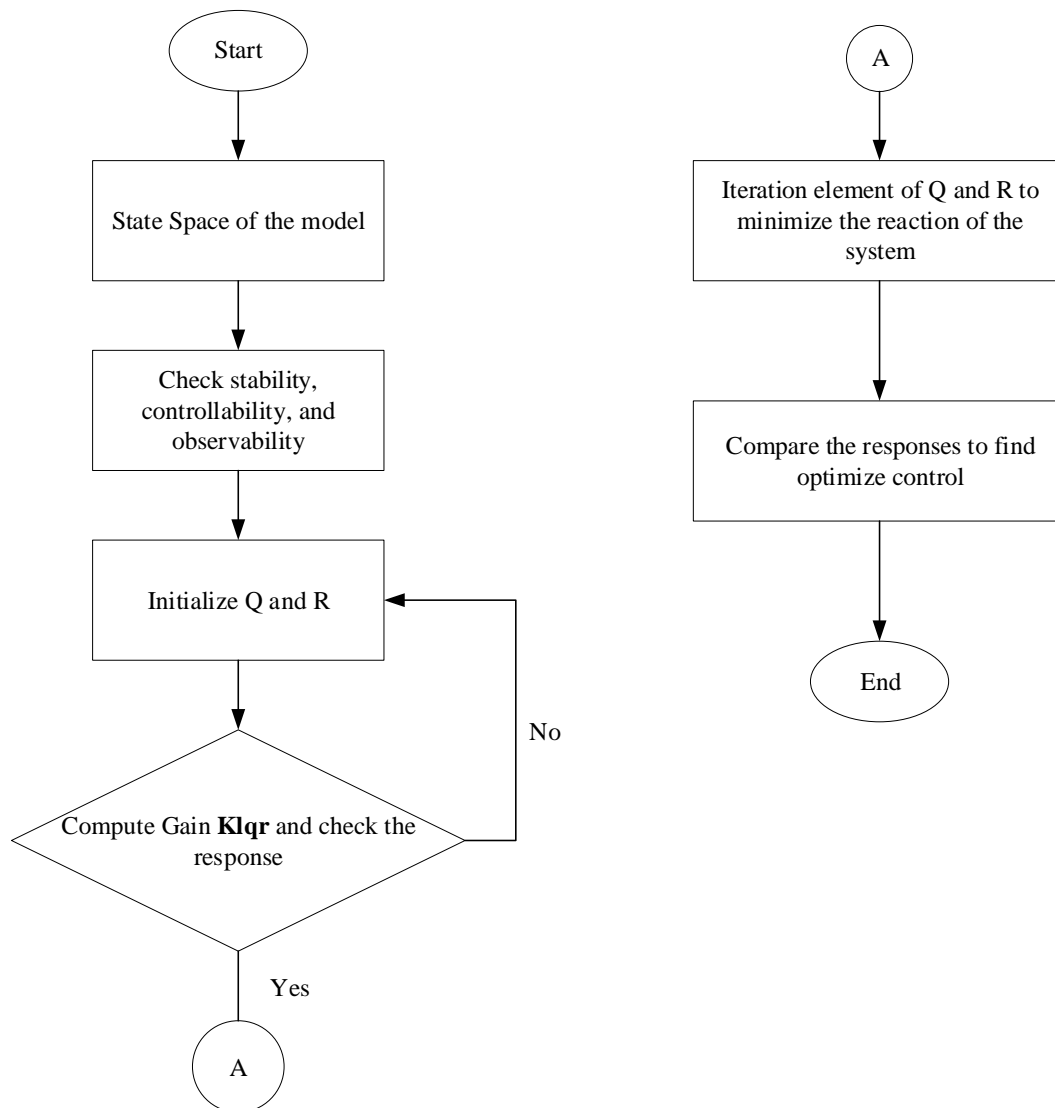
Figure 3.3. The procedure of design LQR controller

3.2 Two-Wheeled Vehicle Models

The design of the gyroscopic two-wheeled vehicle has been designed and produced as illustrated in Figure 3.4. The basic parts of this vehicle consist of the following:

    i.   Base of the vehicle

    ii.   Front and rear wheel

    iii.   Two gyroscopes

    iv.   Two brushless motors and two ESCs to spin the gyroscopic flywheels

v. A DC motors with encoder and motor driver to rotate the gyroscopes

vi. Transmission system (Gears, belts, and pulley)

vii. Microcontroller

viii. Battery
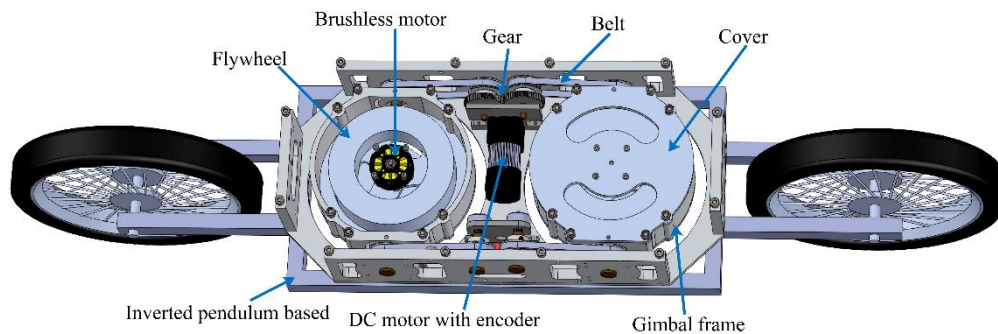
Figure 3.4 The basic parts of the system

In order to require balancing torque to stabilize the vehicle, we could implement with single or double gyroscope. The reason why this project implemented with two gyroscopes instead of one was to have mass properties half of those corresponding to the single gyroscope case. By using smaller sized gyroscopes, the vehicle affected less the symmetry.

3.3 Equation of Motion of Gyroscopic System

There are two approaches to derive the equations of motion of a system: the Newtonian approach and the Lagrangian approach. The Newtonian approach considers each individual component of a system separately. Therefore, the calculation of interacting forces resulting from connections among these sub-parts is required. These connections lead to kinematic constraints. In most cases, these interacting forces can be eliminated by the equations of motion. In this study, the Euler-Lagrange approach is considered for modelling the whole system. The mathematical state-space mode will develop in order to significantly apply feedback controller. Based on the analytical model described in state space, feedback controller and control strategies will be designed in Matlab/Simulink to stabilize the system

Figure 3.5 is a modelling of a two-wheeled vehicle with a double gyroscope that will be derived from the formula with the Lagrange equation.
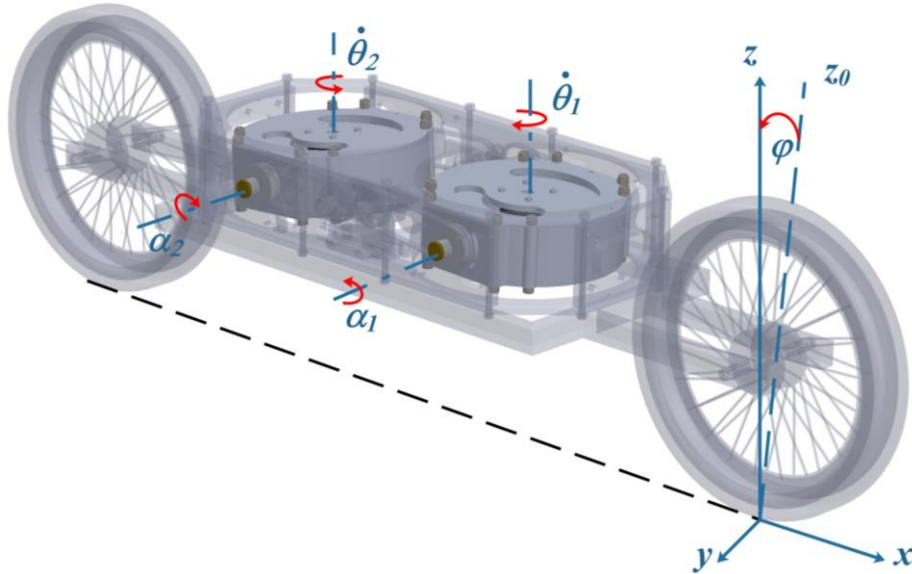
Figure 3.5 Modeling a two-wheeled vehicle with a gyroscopic system

The parameter is written as follows:

1. ω_b: the angular velocity of the body

2. ω_G: the angular velocity of the gimbal

3. ω_{F_i}: the angular velocity of flywheel (i = 1 & 2)

4. m_b: mass of body

5. m_G: mass of gimbal

6. m_{F_i}: mass of flywheel (i = 1 & 2)

7. d_B: the height of the center of gravity of body

8. d_G: the height of the center of gravity of gimbal

9. d_{F_i}: the height of center of gravity of flywheel (i = 1 & 2)

10. ϕ: the main body (pendulum) rotation angle

11. α_i: the angle of gimbal (i = 1 & 2)

The velocity that occurs in a two-wheeled vehicle with a gyroscope can be written as follows:

$$\omega_B = \dot{\phi} x_B \tag{3.3.1}$$

$$\omega_{G_i} = (\dot{\phi}\cos\alpha_i)x_{G_i} + \dot{\alpha}_i y_{G_i} + (\dot{\phi}\sin\alpha_i)z_{G_i} \tag{3.3.2}$$

$$\omega_{F_i} = (\dot{\phi}\cos\alpha_i)x_{F_i} + \dot{\alpha}_i y_{F_i} + (\dot{\phi}\sin\alpha_i)z_{F_i} + \dot{\theta}z_{F_i} \tag{3.3.3}$$

To obtain the system dynamics, an expression for the total kinetic energy and potential energy are required. The total kinetic energy is obtained as the following:

$$T_B = \frac{1}{2}m_B(\dot{\phi}d_B)^2 + \frac{1}{2}I_{B_{xx}}\dot{\phi}^2 \tag{3.3.4}$$

$$T_{G_i} = \frac{1}{2}m_{G_i}(\dot{\phi}d_{G_i})^2 + \frac{1}{2}\left[I_{G_ix}(\dot{\phi}\cos\alpha_i)^2 + I_{G_iy}(\dot{\alpha}_i)^2 + I_{G_iz}(\dot{\phi}\sin\dot{\alpha})^2\right] \tag{3.3.5}$$

$$T_{F_i} = \frac{1}{2}m_{F_i}(\dot{\phi}d_{F_i})^2 + \frac{1}{2}\left[I_{F_ix}(\dot{\phi}\cos\alpha_i)^2 + I_{F_iy}(\dot{\alpha}_i)^2 + I_{F_iz}(\dot{\phi}\sin\alpha_i + \dot{\theta}_i)^2\right] \tag{3.3.6}$$

$$T = T_B + T_{G_1} + T_{G_2} + T_{F_1} + T_{F_2} \tag{3.3.7}$$

where I_{B_x}, I_{G_ix}, I_{G_iy}, I_{G_iy}, I_{F_ix}, I_{F_iy}, and I_{F_iz} are the mass moment inertia for the main body, gimbal frame and flywheel (with i = 1, 2), respectively. The potential energy of each part of the inverted pendulum can be expressed as the following:

$$V_B = m_B g d_B \cos\phi \tag{3.3.8}$$

$$V_G = m_G g d_G \cos\phi \tag{3.3.9}$$

$$V_{F_i} = m_{F_i} g d_{F_i} \cos\phi \tag{3.3.10}$$

$$V = V_B + V_{G_1} + V_{G_2} + V_{F_1} + V_{F_2} \tag{3.3.11}$$

where d_B, d_{G_i} and d_{F_i} are the height of each part measured from the pendulum's pivot point to the center of gravity. The equation of motion by using the Lagrangian equation expressed as:

$$L = T - V$$

$$L = \frac{1}{2} m_B (\dot{\phi} d_B)^2 + \frac{1}{2} I_{Bxx} \dot{\phi}^2 + \frac{1}{2} m_{G_1} (\dot{\phi} d_{G_1})^2$$

$$+ \frac{1}{2} \left[I_{G_1} (\dot{\phi} \cos \alpha_1)^2 + I_{G_1 yy} (\dot{\alpha}_1)^2 + I_{G_{1zz}} (\dot{\phi} \sin \alpha_1)^2 \right]$$

$$+ \frac{1}{2} m_{G_2} (\dot{\phi} d_{G_2})^2$$

$$+ \frac{1}{2} \left[I_{G_{2xx}} (\dot{\phi} \cos \alpha_2)^2 + I_{G_2 yy} (\dot{\alpha}_2)^2 + I_{G_{2zz}} (\dot{\phi} \sin \alpha_2)^2 \right]$$

$$+ \frac{1}{2} m_{F_1} (\dot{\phi} d_{F_1})^2 \qquad (3.3.12)$$

$$+ \frac{1}{2} \left[I_{F_{1xx}} (\dot{\phi} \cos \alpha_1)^2 + I_{F_1 yy} (\dot{\alpha}_1)^2 + I_{F_{1zz}} (\dot{\phi} \sin \alpha_1 + \dot{\theta}_1)^2 \right]$$

$$+ \frac{1}{2} m_{F_2} (\dot{\phi} d_{F_2})^2$$

$$+ \frac{1}{2} \left[I_{F_{2xx}} (\dot{\phi} \cos \alpha_2)^2 + I_{F_2 yy} (\dot{\alpha}_2)^2 + I_{F_{2zz}} (\dot{\phi} \sin \alpha_2 + \dot{\theta}_2)^2 \right]$$

$$- (m_B g d_B \cos \phi + m_{G_1} g d_{G_1} \cos \phi + m_{F_1} g d_{F_1} \cos \phi$$

$$+ m_{G_2} g d_{G_2} \cos \phi + m_{F_2} g d_{F_2} \cos \phi)$$

Apply Lagrange's equations in the form

$$\frac{d}{dt} \left(\frac{\partial L}{\partial \dot{q}_i} \right) - \frac{\partial L}{\partial q_i} = Q_i$$

where the q_i and Q_i are the generalized coordinates and forces for the system, respectively.

- $q_1 = \phi \, \& \, Q_1 = 0$

$$\frac{d}{dt} \left(\frac{\partial L}{\partial \dot{q}_1} \right) - \frac{\partial L}{\partial q_1} = Q_1 \qquad (3.3.13)$$

$$I_{Bxx}\ddot{\phi} + I_{F_1zz}\sin\alpha_1\ddot{\theta}_1 + I_{F_2zz}\sin\alpha_2\ddot{\theta}_2 + I_{F_1zz}\cos^2\alpha_1\ddot{\phi}$$
$$+I_{F_2zz}\cos^2\alpha_2\ddot{\phi} + I_{G_1xx}\cos^2\alpha_1\ddot{\phi} + I_{G_2zz}\cos^2\alpha_2\ddot{\phi}$$
$$+I_{F_1zz}\sin^2\alpha_1\ddot{\phi} + I_{F_2zz}\sin^2\alpha_2\ddot{\phi} + I_{G_1zz}\sin^2\alpha_1\ddot{\phi} + I_{G_2zz}\sin^2\alpha_2\ddot{\phi}$$
$$+m_{F_1}d_{F_1}^2\ddot{\phi} + m_{F_2}d_{F_2}^2\ddot{\phi} + m_{G_1}d_{G_1}^2\ddot{\phi} + m_{G_2}d_{G_2}^2\ddot{\phi} + m_Bd_B^2\ddot{\phi}$$
$$+I_{F_1zz}\cos\alpha_1\dot{\alpha}_1\dot{\theta}_1 + I_{F_2zz}\cos\alpha_2\dot{\alpha}_2\dot{\theta}_2 - m_{F_1}gd_{F_1}\sin\phi$$
$$-m_{F_2}gd_{F_2}\sin\phi - m_{G_1}gd_{G_1}\sin\phi - m_{G_2}gd_{G_2}\sin\phi \qquad (3.3.14)$$
$$-m_Bgd_B\sin\phi - 2I_{F_1xx}\cos\alpha_1\sin\alpha_1\dot{\theta}_1$$
$$-2I_{F_2xx}\cos\alpha_2\sin\alpha_2\dot{\alpha}_2\dot{\theta}_2 + 2I_{F_1zz}\cos\alpha_1\sin\alpha_1\dot{\alpha}_1\dot{\phi}$$
$$+2I_{F_2zz}\cos\alpha_2\sin\alpha_2\dot{\alpha}_2\dot{\phi} - 2I_{G_1xx}\cos\alpha_1\sin\alpha_1\dot{\alpha}_1\dot{\phi}$$
$$-2I_{G_2xx}\cos\alpha_2\sin\alpha_2\dot{\alpha}_2\dot{\phi} + 2I_{G_1zz}\cos\alpha_1\sin\alpha_1\dot{\alpha}_1\dot{\phi}$$
$$+2I_{G_2zz}\cos\alpha_2\sin\alpha_2\dot{\alpha}_2\dot{\phi} = 0$$

- $q_2 = \alpha_1 \ \& \ Q_2 = u_2 = u_{\alpha_1}$

$$\frac{d}{dt}\left(\frac{\partial L}{\partial\dot{q}_2}\right) - \frac{\partial L}{\partial q_2} = Q_2 \qquad (3.3.15)$$

$$I_{F_1yy}\ddot{\alpha}_1 + I_{F_1yy}\ddot{\alpha}_1 + I_{F_1xx}\cos\alpha_1\sin\alpha_1\dot{\phi}^2$$
$$-I_{F_1zz}\cos\alpha_1\sin\alpha_1\dot{\phi}^2 + I_{G_1xx}\cos\alpha_1\sin\alpha_1\dot{\phi}^2$$
$$-I_{G_1zz}\cos\alpha_1\sin\alpha_1\dot{\phi}^2 - I_{F_1zz}\cos\alpha_1\dot{\phi}\dot{\theta}_1 = u_{\alpha_1}$$

- $q_3 = \alpha_2 \ \& \ Q_3 = u_3 = u_{\alpha_2}$

$$\frac{d}{dt}\left(\frac{\partial L}{\partial\dot{q}_3}\right) - \frac{\partial L}{\partial q_3} = Q_3 \qquad (3.3.16)$$

$$I_{F_2yy}\ddot{\alpha}_2 + I_{G_2yy}\ddot{\alpha}_2 + I_{F_2xx}\cos\alpha_2\sin\alpha_2\dot{\phi}^2$$
$$-I_{F_2zz}\cos\alpha_2\sin\alpha_2\dot{\phi}^2 + I_{G_2xx}\cos\alpha_2\sin\alpha_2\dot{\phi}^2$$
$$-I_{G_2zz}\cos\alpha_2\sin\alpha_2\dot{\phi}^2 - I_{F_2zz}\cos\alpha_2\dot{\phi}\dot{\theta}_2 = u_{\alpha_2}$$

- $q_4 = \theta_1 \ \& \ Q_4 = 0$

$$\frac{d}{dt}\left(\frac{\partial L}{\partial\dot{q}_4}\right) - \frac{\partial L}{\partial q_4} = Q_4 \qquad (3.3.17)$$

$$I_{F_1zz}\ddot{\theta}_1 + I_{F_1zz}\sin\alpha_1\ddot{\phi} + I_{F_1zz}\cos\alpha_1\dot{\phi}\dot{\theta}_1 = 0$$

25

- $q_5 = \theta_2 \ \& \ Q_5 = 0$

$$\frac{d}{dt}\left(\frac{\partial L}{\partial \dot{q}_5}\right) - \frac{\partial L}{\partial q_5} = Q_5 \tag{3.3.18}$$

$$I_{F_2zz}\ddot{\theta}_2 + I_{F_2zz}\sin\alpha_2\ddot{\phi} + I_{F_2zz}\cos\alpha_2\dot{\phi}\dot{\theta}_2 = 0$$

Linearization is done to simplify the equation that has been derived so that it is easy to control and observe the dynamic system of the two-wheeled vehicle gyroscopic system. The equations taken in $q_1 = \phi, q_2 = \alpha_1,$ and $q_3 = \alpha_2$ are due to the performance of the vehicle and the two gimbal that will be observed, we obtain the equation of motion is as follow

$$\begin{aligned}
&I_{Bx}\ddot{\phi} + I_{F_1x}\ddot{\phi} + I_{F_2x}\ddot{\phi} + I_{G_1x}\ddot{\phi} + I_{G_2x}\ddot{\phi} + m_{F1}d_{F_1}^2\ddot{\phi} + m_{F2}d_{F_2}^2\ddot{\phi} \\
&+ m_{G1}d_{G_1}^2\ddot{\phi} + m_{G2}d_{G_2}^2\ddot{\phi} + m_Bd_B^2\ddot{\phi} + I_{F_1z}\dot{\alpha}_1\dot{\theta}_1 + I_{F_2z}\dot{\alpha}_2\dot{\theta}_2 \\
&- m_{F_1}gd_{F1}\phi - m_{G_2}gd_{G2}\phi - m_{G_1}gd_{G1}\phi - m_Bgd_B\phi = 0
\end{aligned} \tag{3.3.19}$$

Let

$$M_p = I_{Bx} + I_{F_1x} + I_{F_2x} + I_{G_1x} + I_{G_2x} + m_{F_1}d_{F_1}^2 + m_{F_2}d_{F_2}^2 + m_{G_1}d_{G_1}^2 + m_{G_2}d_{G_2}^2 + m_Bd_B^2$$

$$M_V = m_{F_1}gd_{F_1} + m_{F_2}gd_{F_2} + m_{G_1}gd_{G_1} + m_{G_2}gd_{G_2} + m_Bgd_B$$

$$\ddot{\phi} = \frac{M_V}{M_P}\phi - \frac{I_{F_1z}\dot{\theta}_1}{M_P}\dot{\alpha}_1 - \frac{I_{F_2z}\dot{\theta}_2}{M_P}\dot{\alpha}_2 \tag{3.3.20}$$

$$I_{F_1y}\ddot{\alpha}_1 + I_{G_1y}\ddot{\alpha}_2 - I_{F_1z}\dot{\phi}\dot{\theta}_2 = u_{\alpha_1}$$

$$\ddot{\alpha}_1 = \frac{1}{I_{F_1y} + I_{G_1y}}u_{\alpha_1} + \frac{I_{F_1z}\dot{\theta}_1}{I_{F_1y} + I_{G_1y}}\dot{\phi} \tag{3.3.21}$$

$$I_{F_2y}\ddot{\alpha}_2 + I_{G_2y}\ddot{\alpha}_2 - I_{F_2z}\dot{\phi}\dot{\theta}_2 = u_{\alpha_2}$$

$$\ddot{\alpha}_2 = \frac{1}{I_{F_2y} + I_{G_2y}}u_{\alpha_2} + \frac{I_{F_2z}\dot{\theta}_2}{I_{F_2y} + I_{G_2y}}\dot{\phi} \tag{3.3.22}$$

3.3.1 Gimbal Transmission System Motion Equation

In this study, each gimbal is driven by a single DC motor attached with transmission system. Therefore, the magnitude of rotation of each gimbal has the same value but in the opposite direction. As shown in Figure 3.6, the shaft of the DC motor linked with gear 1, while gear 6 and 7 connected with each gimbal.
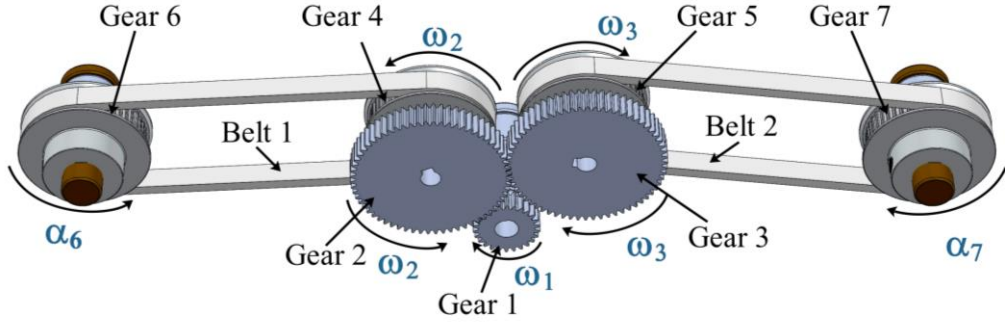
Figure 3.6 gyroscope invert transmission system

The parameters of transmission system are written as the following:

1. J_i: the transmission gear inertia $(i = 1, 2, ..., 7)$

2. R_i: the transmission gear ratio $(i = 1, 2, ..., 7)$

3. $\dot{\omega}_i$: the angular acceleration of the transmission gear $(i = 1, 2, 3, 4)$

4. $\ddot{\alpha}_i$: the angular acceleration of the transmission gear $(i = 6, 7)$

5. $f_{C_g 1}$: the contact force between gear 1 and gear 2

6. $f_{C_g 2}$: the contact force between gear 2 and gear 3

7. $f_{C_b i}$: the pulley and belt contact force $(i = 1, 2, 3, 4)$

8. Ta: is the external force exerted on the gear

Therefore, we obtained the equation of the forces acting on the gimbal. The transmission system by following the free body diagram is shown in Figure 3.7.
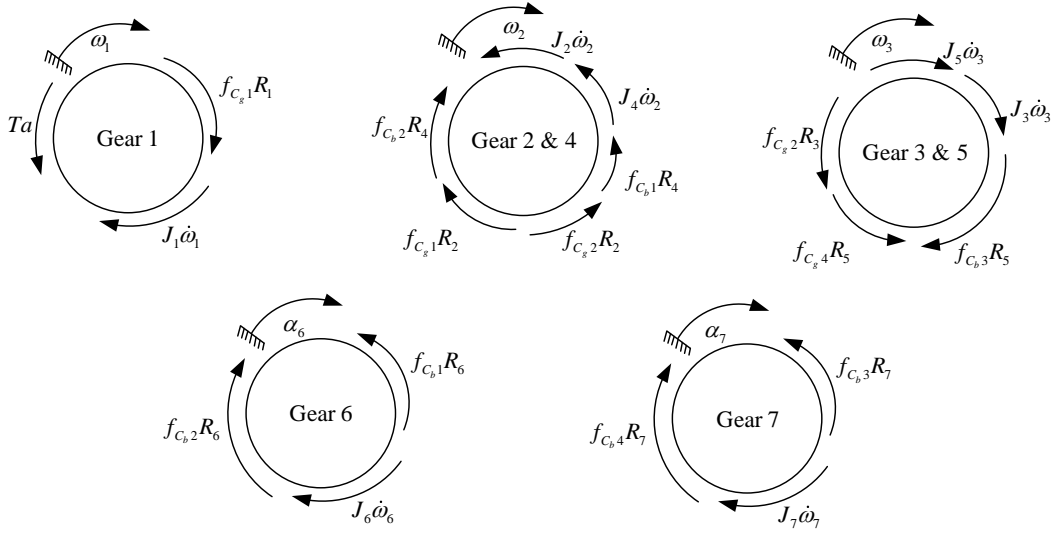
Figure 3.7 Free body diagram of the transmission system on the gyroscope

The transmission equation can be written as follows:

$$J_1\dot{\omega}_1 + f_{C_g1}R_1 = Ta \tag{3.3.23}$$

$$f_{C_g1}R_2 + f_{C_b2}R_4 = f_{C_b1}R_4 + J_4\dot{\omega}_2 + J_2\dot{\omega}_2 + f_{C_b2}R_2 \tag{3.3.24}$$

$$J_5\dot{\omega}_3 + J_3\dot{\omega}_3 + f_{C_b1}R_5 = f_{C_g2}R_3 + f_{C_b4}R_5 \tag{3.3.25}$$

$$J_6\ddot{\alpha}_6 + f_{C_b2}R_6 = f_{C_b1}R_6 \tag{3.3.26}$$

$$J_7\ddot{\alpha}_7 + f_{C_b4}R_7 = f_{C_b3}R_7 \tag{3.3.27}$$

Substitute (3.3.23) and (3.3.26) into (3.3.24), we obtain:

$$\frac{Ta - J_1\dot{\omega}_1}{R_1}R_2 + f_{C_b2}R_4 = \frac{J_6\ddot{\alpha}_6 - f_{C_b2}R_6}{R_6}R_4 + J_4\dot{\omega}_2 + J_2\dot{\omega}_2 + f_{C_g2}R_2 \tag{3.3.28}$$

Substitute (3.3.25) into (3.3.27)

$$J_5\dot{\omega}_3 + J_3\dot{\omega}_3 + \frac{J_7\ddot{\alpha}_7 - f_{C_b4}R_7}{R_7}R_5 = f_{C_g2}R_3 + f_{C_g4}R_5 \tag{3.3.29}$$

For $\dfrac{R_4}{R_6} = 1.5, \dfrac{R_5}{R_7} = 1.5,$ and $\dfrac{R_2}{R_3} = 1$; replaced in (3.3.28) and (3.3.29)

$$\frac{Ta - J_1\dot{\omega}_1}{R_1}R_2 + 1.5f_{C_b2}R_6 = 1.5(J_6\ddot{\alpha}_6 + f_{C_b2}R_6) + J_4\dot{\omega}_2 + J_2\dot{\omega}_2$$
$$+J_5\dot{\omega}_3 + J_3\dot{\omega}_3 + 1.5(J_7\ddot{\alpha}_7 + f_{C_b4}R_7) - 1.5f_{C_b4}R_7 \qquad (3.3.30)$$

For $\dfrac{R_2}{R_1} = N_1, \dfrac{R_3}{R_2} = N_2 = 1,$ and $\dfrac{\dot{\omega}_1}{N_1} = \dot{\omega}_2, \dfrac{\dot{\omega}_1}{N_1 N_2} = \dot{\omega}_3$, substitute into (3.3.30)

$$N_1 T_{a(t)} - 1.5J_6\ddot{\alpha}_6 - 1.5J_7\ddot{\alpha}_7 = \left(\frac{J_4 + J_2 + J_5 + J_3}{N_1} + N_1 J_1\right)\dot{\omega}_1 \qquad (3.3.31)$$

Assumed that the angular acceleration of each gimbal ($\ddot{\alpha}_1$ & $\ddot{\alpha}_2$) is each to the driven gear ($\ddot{\alpha}_6$ & $\ddot{\alpha}_7$). Substitute (3.3.21) and (3.3.22) into (3.3.31)

$$\left(\frac{J_4 + J_2 + J_5 + J_3}{N_1} + N_1 J_1\right)\dot{\omega}_1 = N_1 Ta$$
$$-1.5\left(\frac{J_6}{I_{F_1y} + I_{G_1y}}u_{\alpha_1} + \frac{J_6 I_{F_1z}\dot{\theta}_1}{I_{F_1y} + I_{G_1y}}\dot{\phi}\right) \qquad (3.3.32)$$
$$-1.5\left(\frac{J_7}{I_{F_2y} + I_{G_2y}}u_{\alpha_2} + \frac{J_7 I_{F_2z}\dot{\theta}_2}{I_{F_2y} + I_{G_2y}}\dot{\phi}\right)$$

By comparing the values of each gear in the transmission system, a comparison of input values is obtained $u_{\alpha_1} = 0.8125Ta$ and $u_{\alpha_2} = -0.8125Ta$. Let $\ddot{\alpha}_g = \dot{\omega}_1$

$$\left(\frac{J_4 + J_2 + J_5 + J_3}{N_1} + N_1 J_1\right)\ddot{\alpha}_g =$$
$$\left(N_1 - \frac{1.218J_6}{I_{F_1y} + I_{G_1y}} + \frac{1.218J_7}{I_{F_2y} + I_{G_2y}}\right)Ta \qquad (3.3.33)$$
$$-\left(\frac{1.5J_6 I_{F_1z}\dot{\theta}_1}{I_{F_1y} + I_{G_1y}} + \frac{1.5J_7 I_{F_2z}\dot{\theta}_2}{I_{F_2y} + I_{G_2y}}\right)\dot{\phi}$$

Let $M_n = \left(\dfrac{J_2 + J_3 + J_4 + J_5}{N_1} + N_1 J_1\right)$

We obtain

$$\ddot{\alpha}_g = \left(\frac{N_1 - \dfrac{1.218J_6}{I_{F_1y} + I_{G_1y}} + \dfrac{1.218J_7}{I_{F_2y} + I_{G_2y}}}{M_n} \right) Ta - \left(\frac{\dfrac{1.5J_6 I_{F_1z}\dot{\theta}_1}{I_{F_1y} + I_{G_1y}} + \dfrac{1.5J_7 I_{F_2z}\dot{\theta}_2}{I_{F_2y} + I_{G_2y}}}{M_n} \right) \dot{\phi} \quad (3.3.34)$$

The State-space equation can be written as follows:

$$\dot{x} = Ax + Bu$$

$$\begin{bmatrix} \dot{\phi} \\ \dot{\alpha}_g \\ \ddot{\phi} \\ \ddot{\alpha}_g \end{bmatrix} = \begin{bmatrix} 0 & 0 & 1 & 0 \\ 0 & 0 & 0 & 1 \\ \dfrac{M_V}{M_P} & 0 & 0 & a_{34} \\ 0 & 0 & a_{43} & 0 \end{bmatrix} \begin{Bmatrix} \phi \\ \alpha_g \\ \dot{\phi} \\ \dot{\alpha}_g \end{Bmatrix} + \begin{bmatrix} 0 \\ 0 \\ 0 \\ b_{41} \end{bmatrix} \{Ta\} \quad (3.3.35)$$

That the value of a_{43}, a_{34}, and b_{41} are:

$$a_{43} = -\frac{\dfrac{1.5J_6 I_{F_1z}\dot{\theta}_1}{I_{F_1y} + I_{G_1y}} + \dfrac{1.5J_7 I_{F_2z}\dot{\theta}_2}{I_{F_2y} + I_{G_2y}}}{M_n}$$

$$b_{41} = \frac{N_1 - \dfrac{1.28J_6}{I_{F_1y} + I_{G_1y}} + \dfrac{1.28J_7}{I_{F_2y} + I_{G_2y}}}{M_n}$$

$$a_{34} = -\frac{0.8125 I_{F_1z}\dot{\theta}_1}{M_P} + \frac{0.8125 I_{F_2z}\dot{\theta}_2}{M_P}$$

3.3.2   Model DC Motor Dynamics

In this study, the input torque is needed to apply for turning the gimbal of the gyroscopes. This torque is generated when we apply a certain voltage to the DC motors. In this study, we can directly consider the input of the whole system as the voltage applied to the DC motor. The dynamics of the DC motor which will later be merged with the state-space model. The electric equivalent circuit of the armature and the free body diagram of the rotor are shown in Figure 3.8.
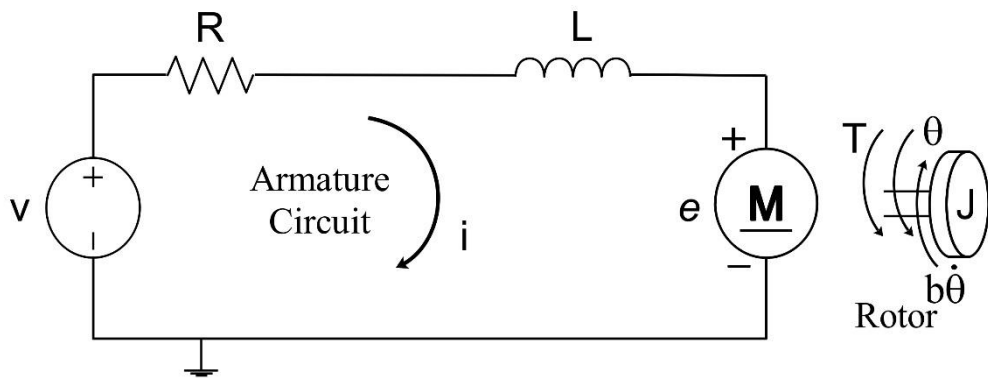
Figure 3.8 The electric equivalent circuit of the armature and rotor

The physical parameters of the model:

1. J: moment inertia of the rotor

2. b: motor viscous friction constant

3. Ke: electromotive force constant

4. Kt: motor torque constant

5. R: electric resistance

6. L: electric inductance

For the mechanical, we obtain the following equation as below based on Newton's 2nd law.

$$T - b\dot{\theta} = J\ddot{\theta} \qquad (3.3.36)$$

In general, the torque generated by a DC motor is proportional to the armature current and the strength of the magnetic field. The motor torque is proportional to only the armature current i by a constant factor K_t as shown in equation (3.3.27).

$$T = K_t i \qquad (3.3.37)$$

Substitute (3.3.37) into (3.3.36), we obtain

$$J\ddot{\theta} + b\dot{\theta} = K_t i \qquad (3.3.38)$$

For the electrical part, we can derive the following governing equation based on Kirchhoff's voltage law.

$$V - Ri - L\frac{di}{dt} - V_{emf} = 0 \tag{3.3.39}$$

The back emf, V_{emf}, is proportional to the angular velocity of the shaft by a constant factor K_e.

$$V_{emf} = K_e\dot{\theta} \tag{3.3.40}$$

Substitute (3.3.40) into (3.3.39), we obtain:

$$V - Ri - L\frac{di}{dt} - K_e\dot{\theta} = 0 \tag{3.3.41}$$

In the state-space form, the equation above can be expressed by choosing the rotational speed and electrical current as of the state variables.

$$\frac{d}{dt}\begin{bmatrix} \dot{\theta} \\ i \end{bmatrix} = \begin{bmatrix} -\dfrac{b}{J} & \dfrac{K_t}{J} \\ -\dfrac{K_e}{L} & -\dfrac{R}{L} \end{bmatrix}\begin{bmatrix} \dot{\theta} \\ i \end{bmatrix} + \begin{bmatrix} 0 \\ \dfrac{1}{L} \end{bmatrix}V \tag{3.3.42}$$

$$y = \begin{bmatrix} 1 & 0 \end{bmatrix}\begin{bmatrix} \dot{\theta} \\ i \end{bmatrix} \tag{3.3.43}$$

Where V is the voltage that will supply to the motor in order to produce the desired torque and $y = \dot{\theta}$ is the angular velocity output of the DC motor. Thus, the angular velocities of the DC-motors must be equal with the respective precession rates of the gyroscopes $y = \dot{\theta} = \dot{\alpha}_g$.

The angular velocity of the inertia connected to the motor is given by

$$\frac{d\dot{\theta}}{dt} = \frac{1}{J}T \tag{3.3.44}$$

Therefore, the torque that will be applied on the gyroscopes will be

$$T = Ta = -b\dot{\theta} + K_t i \tag{3.3.45}$$

3.3.1 State space full system

Although a nonlinear model of the system is derived and verified in the previous section, and the linear model around an operating point is also obtained. In order to synthesize the controller, state space full system dynamic is required. A state-space formulation allows one to get more information about the system than the input/output formulation, which is described only by a transfer function. Specifically, if A, B, C, and D are known, then the internal states x(t) can be computed in addition to the input u(t) and output y(t). Since the operating point of the system is the upright position and the gimbal angles are zero, the flywheels are rotating at a constant speed in the inverse direction of 6000 rpm. The new state vector will be $\begin{bmatrix} \phi & \dot{\phi} & \alpha_g & \dot{\alpha}_g & i \end{bmatrix}$ and the state space model of the full system described as the following:

$$\dot{x} = Ax + Bu$$

$$
\begin{bmatrix} \dot{\phi} \\ \dot{\alpha}_g \\ \ddot{\phi} \\ \ddot{\alpha}_g \\ \dfrac{di}{dt} \end{bmatrix} =
\begin{bmatrix}
0 & 0 & 1 & 0 & 0 \\
0 & 0 & 0 & 1 & 0 \\
\dfrac{M_V}{M_P} & 0 & 0 & a_{34} & 0 \\
0 & 0 & a_{43} & -a_{44} & a_{45} \\
0 & 0 & 0 & -\dfrac{K_e}{L} & -\dfrac{R}{L}
\end{bmatrix}
\begin{bmatrix} \phi \\ \alpha_g \\ \dot{\phi} \\ \dot{\alpha}_g \\ i \end{bmatrix} +
\begin{bmatrix} 0 \\ 0 \\ 0 \\ 0 \\ \dfrac{1}{L} \end{bmatrix} [V]
\qquad (3.3.46)
$$

Where

$$a_{34} = -\frac{0.8125 I_{F_1 z} \dot{\theta}_1}{M_P} + \frac{0.8125 I_{F_2 z} \dot{\theta}_2}{M_P}$$

$$a_{44} = b \times \frac{N_1 - \dfrac{1.28 J_6}{I_{F_1 y} + I_{G_1 y}} + \dfrac{1.28 J_7}{I_{F_2 y} + I_{G_2 y}}}{M_n}$$

$$a_{45} = K_t \times \frac{N_1 - \dfrac{1.28 J_6}{I_{F_1 y} + I_{G_1 y}} + \dfrac{1.28 J_7}{I_{F_2 y} + I_{G_2 y}}}{M_n}$$

where

- $x_1 = \phi$ is the roll angle of the vehicle

- $x_2 = \alpha_g$ is the motor shaft angle

- $x_3 = \dot{\phi}$ is the roll rate

- $x_4 = \dot{\alpha}_g$ is the motor shaft angle rate

- $x_5 = i$ is the current in the motor's armature

The whole procedure of the closed loop system with the control scheme is illustrated in Figure 3.9.
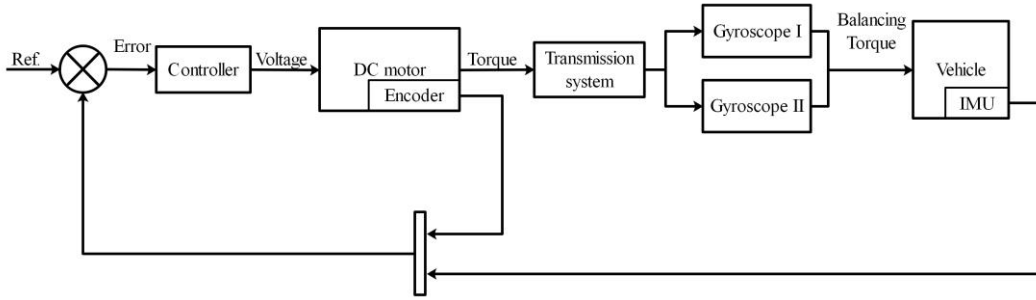
Figure 3.9. Procedure of the close-loop system

3.3.2 Stability, controllability and observability check

Before designing the controller, it is necessary to check the controllability and observability of the open-loop system. The parameters of the gyroscopic two-wheeled vehicle are defined in Table 3.1. These values were used to model the dynamics of the physical system and the controllers.

Table 3.1: Gyroscopic two-wheeled vehicle parameter

Parameter	Symbol	Value (Unit)
Mass of the body, gimbal and flywheel	$[m_B, m_{G_{1,2}}, m_{F_{1,2}}]$	$[5.306, 1.106, 0.71](kg)$
Mass moment inertia of the body	$[I_{B_x}, I_{B_y}, I_{B_z},]$	$[0.248, 0.260, 0.261](kg.m^2)$
Mass moment inertia of the gimbal	$[I_{G_x}, I_{G_y}, I_{G_z}]$	$[0.198, 0.172, 0.332] \times 10^{-3}(kg.m^2)$

Mass moment inertia of the flywheel	$\left[I_{F_x}, I_{F_y}, I_{F_z}\right]$	$[0.877, 0.877, 1.642]$ $\times 10^{-7}(kg.m^2)$
Height of each part at COG	$\left[d_B, d_{G_{1,2}}, d_{G_{1,2}}\right]$	$[0.152, 0.165, 0.171](m)$
Angular velocity of the flywheel	$\left[\dot{\theta}_1, \dot{\theta}_2\right]$	$[628.31, -628.31](rad/s)$
Mass moment inertia of each gear	$\left[J_1, J_{2,3}, J_{6,7}\right]$	$[0.025, 0.539, 0.266]$ $\times 10^{-5}(kg.m^2)$
The electric resistance	R	$1.9(\Omega)$
The electric inductance	L	$65 \times 10^{-6}(H)$
The motor viscous friction constant	b	$10^{-3}(Nm)$
The moment inertia of the rotor	J	$5.7 \times 10^{-7}(kg.m^2)$
The motor torque constant	K_t	$0.023 \times 10^{-3}(V/rad/s)$
The back emf constant	K_e	$0.023 \times 10^{-3}(V/rad/s)$

3.3.2.1 Stability

The stability of a system can be defined with respect to a given equilibrium point in state space. If the initial state x_0 is selected at an equilibrium state $\bar{x}$ of the system, then the state will remain at $\bar{x}$ for all future time. When the initial state is selected close to an equilibrium state, the system might remain close to the equilibrium state or it might move away.

Numerically, we can determine the stability of a state space model by finding the eigenvalues of the state space A matrix. If all of the eigenvalues are negative, then the system is stable; if any single eigenvalue is positive, the system is unstable. Mathematically, the eigenvalues of the matrix are found from the roots of the characteristic polynomial:

$$\det(\lambda I - A) = 0 \qquad (3.3.47)$$

where λ is known as an eigenvalue, and I is the identify matrix.

$$
\begin{bmatrix} \lambda_1 & 0 & 0 & 0 & 0 \\ 0 & \lambda_2 & 0 & 0 & 0 \\ 0 & 0 & \lambda_3 & 0 & 0 \\ 0 & 0 & 0 & \lambda_4 & 0 \\ 0 & 0 & 0 & 0 & \lambda_5 \end{bmatrix} - \begin{bmatrix} 0 & 0 & 1 & 0 & 0 \\ 0 & 0 & 0 & 1 & 0 \\ 58 & 0 & 0 & -4 & 0 \\ 0 & 0 & 0 & -343 & 4600 \\ 0 & 0 & 0 & -0.3538 & -29231 \end{bmatrix}
$$

$$
= \begin{bmatrix} \lambda_1 & 0 & -1 & 0 & 0 \\ 0 & \lambda_2 & 0 & -1 & 0 \\ -58 & 0 & \lambda_3 & 4 & 0 \\ 0 & 0 & 0 & \lambda_4 + 343 & -4600 \\ 0 & 0 & 0 & 0.3538 & \lambda_5 + 29231 \end{bmatrix}
$$

(3.3.48)

The roots can be found using the quadratic formula

$$
\lambda = \begin{bmatrix} \lambda_1 \\ \lambda_2 \\ \lambda_3 \\ \lambda_4 \\ \lambda_5 \end{bmatrix} = \begin{bmatrix} -3.8027 \\ -0.0451 \\ -0.0031 \\ -0.001 \\ -0.0006 \end{bmatrix} \times 10^4
$$

All of the eigenvalues are negative; thus, the system is stable.

3.3.2.2 Controllability

A system is said to be controllable if all the states are completely controllable. A system can also be considered as controllable, if every state of system can be exercised control in such a manner that they are transferred from an initial state to desired state in some finite time.

The state $x(t)$ at $t=0$ is said to controllable, if the state can be driven to a desired state $x(tf)$ in some finite time $t = tf$ by application of continuous control input $u(t)$. The controllable matrix Q_c is derived as

$$
Q_c = \begin{bmatrix} B & AB & A^2B & \dots & A^{n-1}B \end{bmatrix}
$$
$$
|Q_c| \neq 0 \, and \, rank(Q_c) = n
$$

(3.3.49)

The controllability matric is calculated, and it is seen that it does not lose rank. Therefore, the system is controllable.

3.3.2.3 Observability

A system is said to be observable if the state can be determined from the knowledge of the input u(t) and the output y(t) over a finite interval of time.

The state $x(t_0)$ at $t = t_0$ for a system is said to be observable if a desired finite time $t = tf = t_0$, knowledge of input u(t) and output y(t) over the interval $t_0 < t < tf$ can be calculated. The observable matrix Q_o is derived as

$$Q_o = \begin{bmatrix} C & CA & CA^2 & \dots & CA^{n-1} \end{bmatrix}^T$$
$$|Q_o| \neq 0 \, and \, rank(\mathbf{Q}_o) = n$$

(3.3.50)

The observability matric is calculated, and it is seen that it does not lose rank. It is possible to observe all the states.

CHAPTER 4
CONTROL DESIGN

In this chapter two different control techniques are studied. The purposes of each control strategy, the mathematical model describing the physical system is accordingly considered. PID and LQR are developed to validate the two-wheeled vehicle, and the SimMechanics model is built to verify nonlinear model.

4.1 Cascade PID controller

In this section the design of the cascade PID controller is presented. A simple control algorithm such as PID can be used to generated the closed loop responses [20]. The PID controller refers to a particular action taken on the error. The error is then used to adjust some input to the process in order to its defined set point.

In control problems where we have single input and multiple measurement signals, cascade control is a reasonable choice. In advance, we know that when the roll angle ϕ of the vehicle approached to equilibrium, the roll rate $\dot{\phi}$ also tended to zero. So, the roll angle ϕ will be the first control variable. Meanwhile we would keep the motor shaft angles α_g as close to zero as possible, so the gyroscopes will have enough space to process and generate the stabilizing counter-torque. Consequently, the shaft angle α_g is the second control variable.
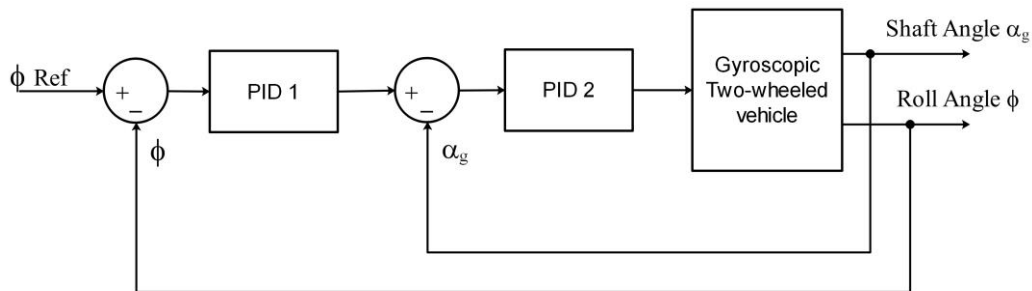
Figure 4.1. PID control scheme

The PID control scheme for the system for the system is shown in Figure 4.1. Two PID controllers are used to control the gyroscopic two-wheeled vehicle. The PID controller in the outer loop minimizes the roll angle ϕ and generates

reference for the inner loop (shaft angle α_g). Since the two flywheels spin at a constant speed in opposite direction, the gimbal angles α_1 and α_2 are moved to produce balancing torque on the horizontal axis.

It is important to determine appropriate parameters to guarantee stability and system performance. There are several methods for tuning PID parameters. However, in this study the six parameters of PID controller values are computed by trial and error.

- Proportional: Error multiplied by a gain, K_P. This is an adjustable amplifier. In many systems K_P is responsible for process stability. Too low and the PV can drift away. Too high and the PV can oscillate.

- Integral: The integral of error multiplied by a gain, K_I. In many systems K_I is responsible for driving error to zero, but to set K_I too high is to invite oscillation or instability.

- Derivative: The rate of change of error multiplied by a gain, K_D. In many systems K_D is responsible for system response. Too high and the PV will oscillate. Too low and the PV will respond sluggishly.

The way to tune the cascade PID controllers is the following. We first tuned the inner loop while having the outer loop in manual mode (open loop). Then, considering the inner loop as part of the plant, we closed and tuned the outer loop. We keep the inner loop at least five times faster than the outer one, so the inner is fast enough to keep the vehicle stable.

Table 4.1 shows different six PID settings that will apply to evaluate the performance of each cascade controller. The cascade PID controller was designed and tuned, which reduced overshoot and minimized settling time of the response.

Table 4.1: Cascade PID parameter with different settings

Case	Loop	Kp	Ki	Kd
1	Outer	1.2	25	1

	Inner	22	0	0
2	Outer	1.2	45	3.3
	Inner	22	0	0.02
3	Outer	1.2	15	1.3
	Inner	22	0.8	0.2
4	Outer	1.5	30	1.2
	Inner	25	1	1.1
5	Outer	1.5	25	1.5
	Inner	22	0.5	0
6	Outer	2	35	3
	Inner	25	0.05	0.05
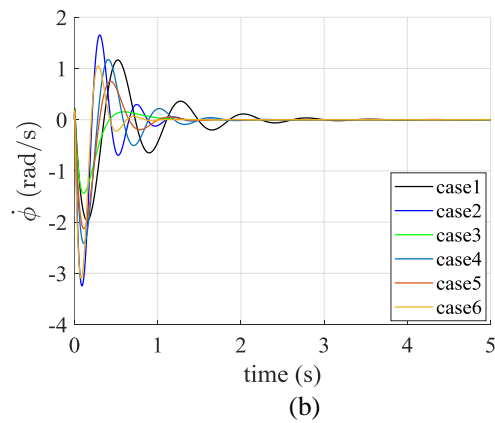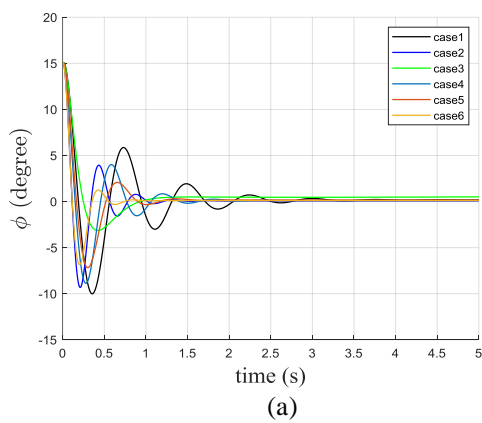
Figure 4.2. Cascade PID response of: (a) roll displacement (b) roll rate
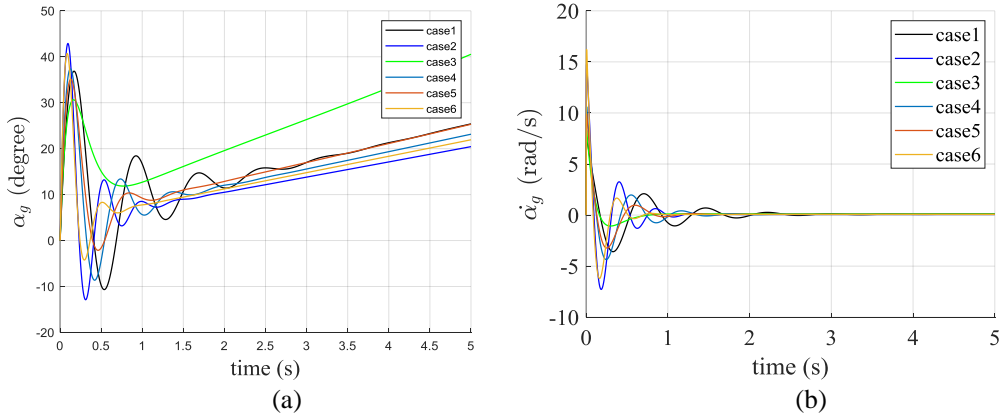
Figure 4.3. Cascade PID response of: (a) shaft displacement (b) shaft rate

In this comparison stage, we have ignored the external disturbances. Figure 4.2 and Figure 4.3 illustrate the performance of each setting so that we can obtain a comparison on the effect of each PID gain. To prevent the shaft motor reaching close to the boundaries of the precession angles $(-45^{\circ}, 45^{\circ})$, we initialized our vehicle from a tilted position that never exceeded the range $(-15^{\circ}, 15^{\circ})$. When the setting is given in case 1 where a P controller for the inner loop, the response of the vehicle and the shaft is more oscillation than the other and the maximum amplitude for the vehicle is highest. In case 2, a PD controller is used in the inner loop, we noted that the maximum amplitude for the shaft motor is highest. However, the vehicle still takes time to reduce oscillation. The vehicle and the vehicle angular velocity take smallest amplitude when the setting is given in case 3, but the shaft motor is for different from the other. The vehicle takes the shortest time to return to the equilibrium position when the setting is given in case 6.

However, all setting of the cascade PID controller not only cannot keep the shaft motor close to zero position, but the shaft motor remains rotating. In general, not only we want to stabilize the vehicle on its upright position, but we also want to drive the gyroscopes to the zero position as fast as possible, so they can offset disturbances that might happen. However, if the gimbal angle were not returned to zero after stabilizing the vehicle then the gyro would not be capable of producing its maximum reaction torque for the next disturbance introduced into the system which could possibly not be enough to stabilize the vehicle.

41

4.2   Linear Quadratic Regulation (LQR) controller

In this section, LQR controllers will be designed, based on the analytical model described in equation (3.3.46). Given that we can full access the state vector, but not only on the measurable states. In order to disable some problems that faced by PID controller, the other type of control methods can be developed such as Linear-Quadratic Regulator (LQR) optimal control. LQR is a control scheme that gives the best possible performance with respect to some given measure of performance. The performance measure is a quadratic function composed of state vector and control input.

Linear Quadratic Regulator (LQR) is the optimal theory of pole placement method. LQR algorithm defines the optimal pole location based on two cost function. To discover the optimal gains, one should define the optimal performance index firstly and then solve algebraic Riccati equation. LQR does not have any specific solution to identify the cost function to obtain the optimal gains and the cost function should be defined in iterative manner. LQR is a control scheme that provides the best possible performance with respect to some given measure of performance. The LQR design problem is to design a state feedback controller K such that the objective function J is minimized. In this method a feedback gain matrix is designed which minimizes the objective function in order to achieve some compromise between the use of control effort, the magnitude, and the speed of response that will guarantee a stable system. The LQR problem rests upon the following three assumptions [21]:

- All the states $x(t)$ are available for feedback, i.e. it can be measured by sensors etc.
- The system is stabilizable which means that all of its unstable modes are controllable (see in 3.3.2).
- The system is detectable having all its unstable modes observable (see in 3.3.2).

42
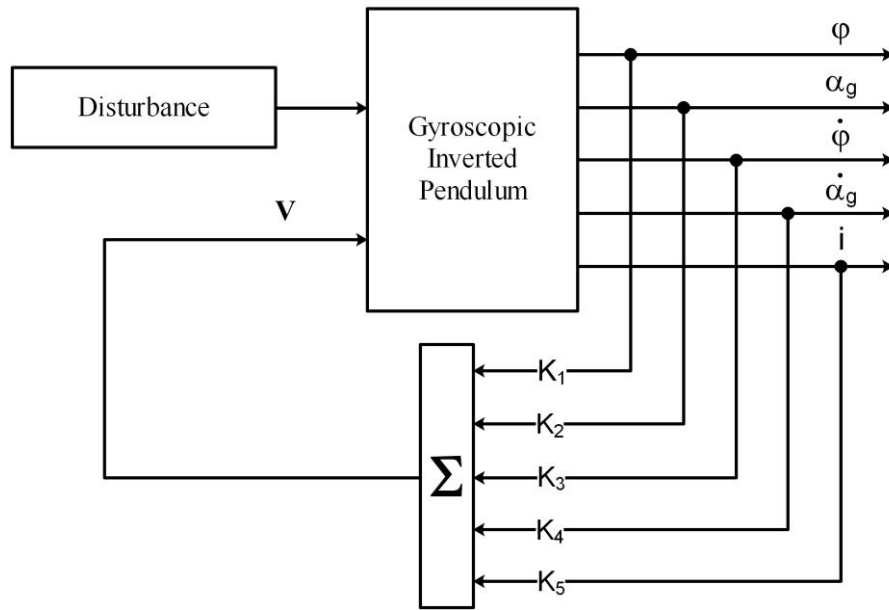
Figure 4.4. LQR controller scheme

Figure 4.4 illustrates the closed loop system with the LQR controller scheme. LQR design is a part of what in the control area is called optimal control. This regulator provides an optimal control law for a linear with quadratic performance index yielding a cost function on the form

$$J = \int_0^\infty x^T(t)Qx(t) + u^T(t)Ru(t)dt \qquad (4.2.1)$$

where $Q = Q^T$ and $R = R^T$ are weight parameters that penalize the states and the control effort, respectively. These matrices are therefore controller tuning parameters. It is crucial that Q must be chosen in accordance to the emphasize we want to give the response of certain states, or in the word; how we will penalize the states. Likewise, the chosen value(s) of R will penalize the control effort u. Hence, in an optimal control problem the control system seeks to maximize the return from the system with minimize the return from system with minimum cost. In the LQR design, the system has a mathematical solution that yields an optimal control law because of the quadratic performance index of the cost function.

$$u(\text{t}) = -Kx(t) \qquad (4.2.2)$$

where u is the control input and K is the gain given as $K = R^{-1}B^TS$. And P can be found by solving the continuous time algebraic Riccati equation:

43

$$A^T P + PA - PBR^{-1}B^T P + Q = 0 \qquad (4.2.3)$$

$$\begin{bmatrix} 0 & 0 & 58 & 0 & 0 \\ 0 & 0 & 0 & 0 & 0 \\ 1 & 0 & 0 & 0 & 0 \\ 0 & 1 & -3 & -343 & -0.3538 \\ 0 & 0 & 0 & 4600 & -2.9231 \end{bmatrix} \begin{bmatrix} P_{11} & P_{12} & P_{13} & P_{14} & P_{15} \\ P_{21} & P_{22} & P_{23} & P_{24} & P_{25} \\ P_{31} & P_{32} & P_{33} & P_{34} & P_{35} \\ P_{41} & P_{42} & P_{43} & P_{44} & P_{45} \\ P_{51} & P_{52} & P_{53} & P_{54} & P_{55} \end{bmatrix}$$

$$+ \begin{bmatrix} P_{11} & P_{12} & P_{13} & P_{14} & P_{15} \\ P_{21} & P_{22} & P_{23} & P_{24} & P_{25} \\ P_{31} & P_{32} & P_{33} & P_{34} & P_{35} \\ P_{41} & P_{42} & P_{43} & P_{44} & P_{45} \\ P_{51} & P_{52} & P_{53} & P_{54} & P_{55} \end{bmatrix} \begin{bmatrix} 0 & 0 & 1 & 0 & 0 \\ 0 & 0 & 0 & 1 & 0 \\ 58 & 0 & 0 & -4 & 0 \\ 0 & 0 & 0 & -343 & 4600 \\ 0 & 0 & 0 & -0.3538 & -29231 \end{bmatrix}$$

$$- \begin{bmatrix} P_{11} & P_{12} & P_{13} & P_{14} & P_{15} \\ P_{21} & P_{22} & P_{23} & P_{24} & P_{25} \\ P_{31} & P_{32} & P_{33} & P_{34} & P_{35} \\ P_{41} & P_{42} & P_{43} & P_{44} & P_{45} \\ P_{51} & P_{52} & P_{53} & P_{54} & P_{55} \end{bmatrix} \begin{bmatrix} 0 \\ 0 \\ 0 \\ 0 \\ 15380 \end{bmatrix} [r_{11}] \begin{bmatrix} 0 \\ 0 \\ 0 \\ 0 \\ 15380 \end{bmatrix}^T \begin{bmatrix} P_{11} & P_{12} & P_{13} & P_{14} & P_{15} \\ P_{21} & P_{22} & P_{23} & P_{24} & P_{25} \\ P_{31} & P_{32} & P_{33} & P_{34} & P_{35} \\ P_{41} & P_{42} & P_{43} & P_{44} & P_{45} \\ P_{51} & P_{52} & P_{53} & P_{54} & P_{55} \end{bmatrix}$$

$$+ \begin{bmatrix} q_{11} & 0 & 0 & 0 & 0 \\ 0 & q_{22} & 0 & 0 & 0 \\ 0 & 0 & q_{33} & 0 & 0 \\ 0 & 0 & 0 & q_{44} & 0 \\ 0 & 0 & 0 & 0 & q_{55} \end{bmatrix} = 0$$

The process of minimizing of the cost function therefore involves to solve this equation, which is will be done with the use of MATLAB function LQR. In this study the parameters in Q was initially chosen

$$Q = \begin{bmatrix} q_1 & 0 & 0 & 0 & 0 \\ 0 & q_2 & 0 & 0 & 0 \\ 0 & 0 & 1 & 0 & 0 \\ 0 & 0 & 0 & 1 & 0 \\ 0 & 0 & 0 & 0 & 1 \end{bmatrix} \qquad (4.2.4)$$

and the control weight of the performance index R was set to 1.

Here we can see that the chosen values in Q result in a relatively effect penalty in the states x_1 and x_2. This means that if x_1 and x_2 are large, the large values in Q will amplify the effect of x_1 and x_2 in the optimization problem. Since

the optimization problem are to minimize J, the optimal control u must force has states x_1 and x_2 to be small (which make sense physically since x_1 and x_2 represent the position of the vehicle and the angle of the gimbal, respectively). These values must be modified during subsequent iterations to achieve as good response as possible (refer to the next section for results). On the other hand, the small R relative to the max values in Q involves very low penalty on the control effort u in the minimization of J, and the optimal control u can be large. For this small R, the gain K can then be large resulting in a faster response. In the physical world this might involve instability problems, especially in systems with saturation [21]. To obtain good matrix gain K, the iteration the elements q_1 and q_2 in matrix Q are conducted.

4.2.1 Iteration by set initial position of the vehicle

The goal of the LQR tuning is to vary the parameters ϕ and α_g such as to minimize the cost [22]. In order to tune the good optimal control, the iteration the elements q_1 and q_2 in matrix Q are conducted in state space linearize model. By set the initial position of the vehicle angle ϕ at 15°, We executed the iteration LQR algorithm 25 times. In particular, the algorithm was terminated after a fixed number of $q_{1,min}$ and $q_{2,min} = 1$ to $q_{1,max}$ and $q_{2,max} = 500$ with the increasement 125.75. In order to evaluate the performance of each resulting controller, we simulated each one 5 times in closed-loop on the linear system. At every iteration, a new controller is obtained in loop and plotted to evaluate the performance of each controller. Figure 4.5 and Figure 4.6 visualize the iteration results when the controller brings the vehicle from initial position 15° to the upright position and we compare the performance and the settling time to find the optimization. Based on these figures, we can demonstrate that the response of the vehicle and the shaft motor are strongly affect by the q_2. The results show that the iteration algorithm resulted in improved controllers for each increasement of q_2 while the q_1 is small affect the controller.
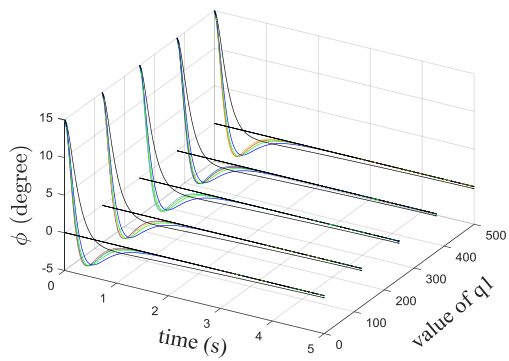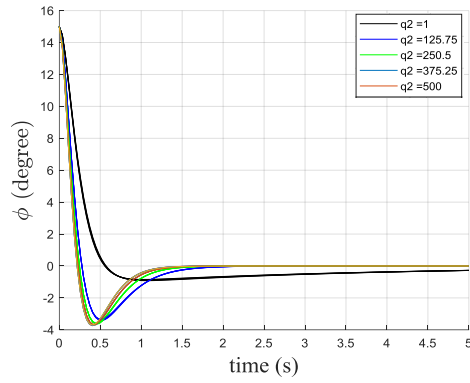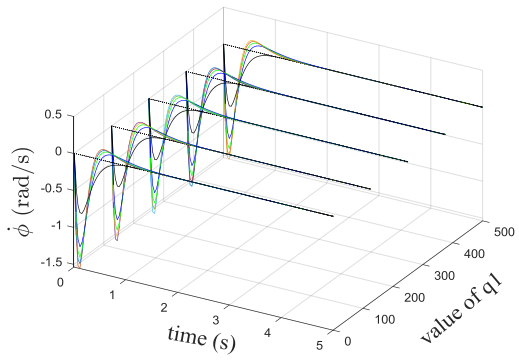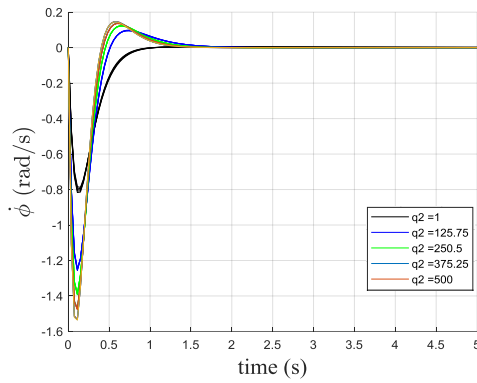
Figure 4.5. The effect of the iteration with: (a) roll angle 3D view, (b) roll angle front view, (c) roll rate 3D view, and (d) roll rate front view
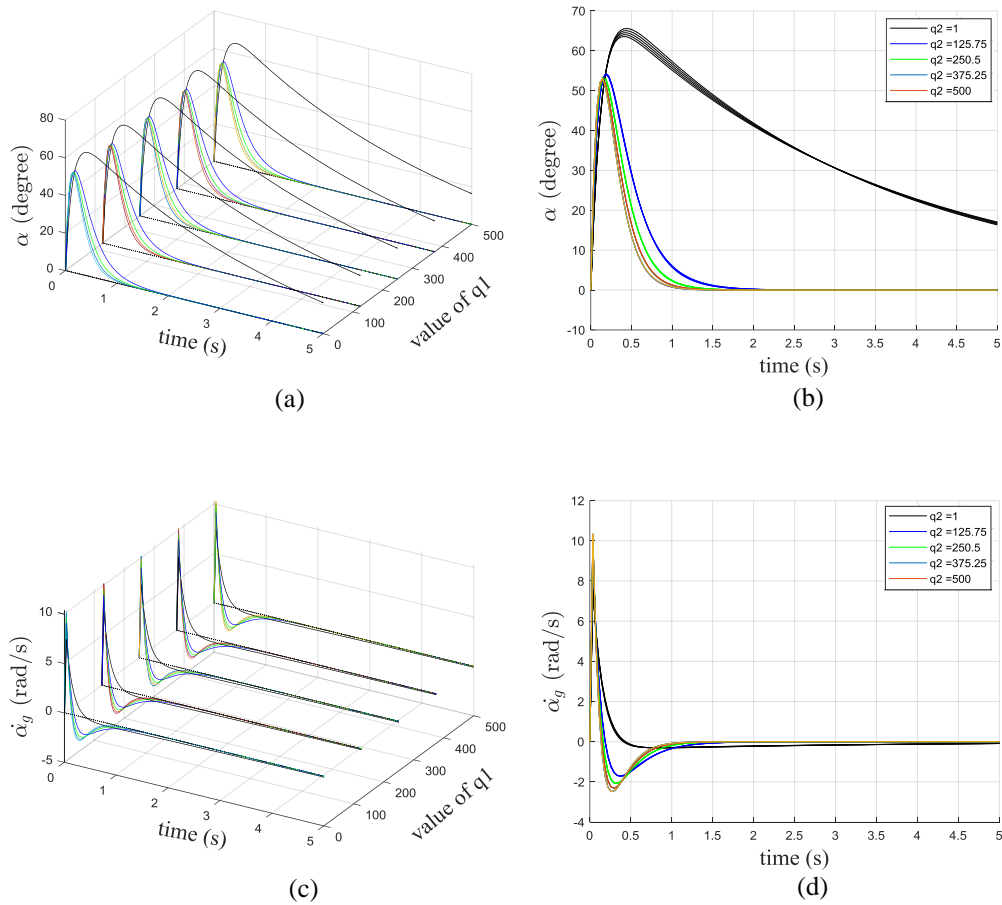
Figure 4.6. The effect of the iteration with the shaft angle: a) 3D view and b) front view

4.2.2   Iteration by apply disturbance to the vehicle

To obtain more efficient LQR controller in order to minimize the objective function, a pre-design LQR controller visualized the performance of the iteration methods. The idea is to display the optimal values of the weighting matrices of LQR controller with respect to an impulse disturbance. Therefore, the weights of states related with shaft angle and vehicle angle are estimated to find the optimal responses. Base on Figure 4.5 and Figure 4.6, we noted that all values of q_1 and q_2 from 1 to 500 could bring the vehicle and the shaft motor back to the upright position. Then we use these ranks of q_1 and q_2 to observe the ability for reject disturbance. In this case, the vehicle is initially at upright position, and later we apply an unwanted input which affect our plant (vehicle) at 3s during balancing.

47

For the simulation study, we use a linearized model, which can be regarded as an abstraction of the nonlinear platform.

Results in graph of the Figure 4.7 show the maximum angle of the vehicle and the shaft motor and the velocity of the shaft motor. The graphical results obtained by the iteration two elements of Q matrix with angular displacement vehicle and shaft motor and angular velocity of shaft motor, respectively. To verify the effectiveness of the improved the optimized LQR controller, the controller has benchmarked on the linear model. The graphs were obtained by uniformly gridding the parameter space, angular displacement with each grid point (q_1 and q_2), and evaluating the maximum angle from simulation data. Depend on the graphs, we can evaluate that the response of the impulse disturbance is strongly affect by the q_1, while the q_1 is small affect the controller. Moreover, the angular velocity of the shaft motor increased because it keeps the vehicle and the motor shaft in small angle due to the control system design process.

(a)

(b)

(c)
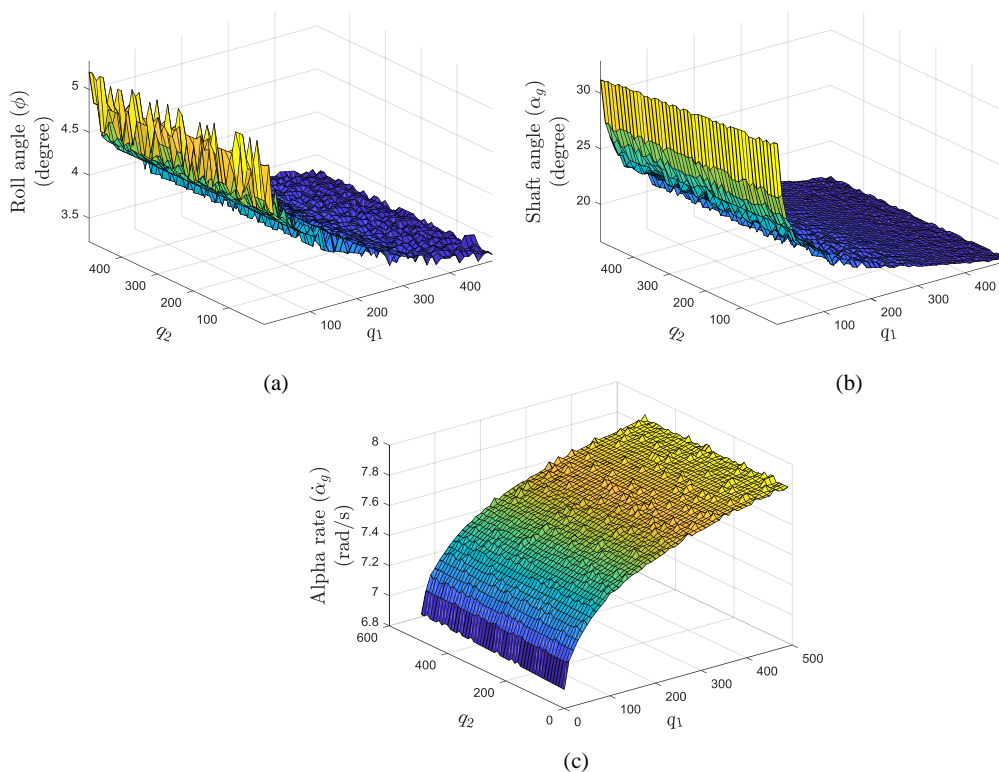
Figure 4.7. The effect of weight that associated with the maximum reaction of: a) vehicle, b) shaft motor, and c) shaft rate

Table 4.2: LQR weight parameter with different settings

Case	Matrix Q	Matrix R
1	$diag(100\ 100\ 1\ 1\ 1)$	[1]
2	$diag(100\ 200\ 10\ 1\ 10)$	[2]
3	$diag(300\ 250\ 10\ 10\ 1)$	[3]
4	$diag(270\ 350\ 1\ 10\ 10)$	[4]
5	$diag(350\ 450\ 10\ 10\ 10)$	[5]

In order to evaluate the robustness of the controllers, the obtained state-feedback controller then applied to a non-linear model developed using Simscape Multibody. Further, the effect of state weighting is studied for five different cases with nonlinear. Table 4.2 shows the weighting matrices to validate and compare the response of each design controller. While Figure 4.8 and Figure 4.9 show the comparison of the time response of the vehicle angle, vehicle angular velocity, shaft angle and shaft angular velocity from an initial position 15° of the vehicle.

When the weighting is given in case 4, the maximum amplitude both for vehicle angle and shaft motor angle are the smallest among other cases. Moreover, the vehicle takes longest time to return to the equilibrium position. The vehicle and the shaft motor take the shortest time to return to the equilibrium position when the weighting is given in case 2, but shaft motor angular velocity for this case is very high. In case 5, largest weights for both state weight matrix Q and input weight R are given, but both the vehicle and the motor shaft return to the equilibrium position longer if compare to case 1 and case 2.
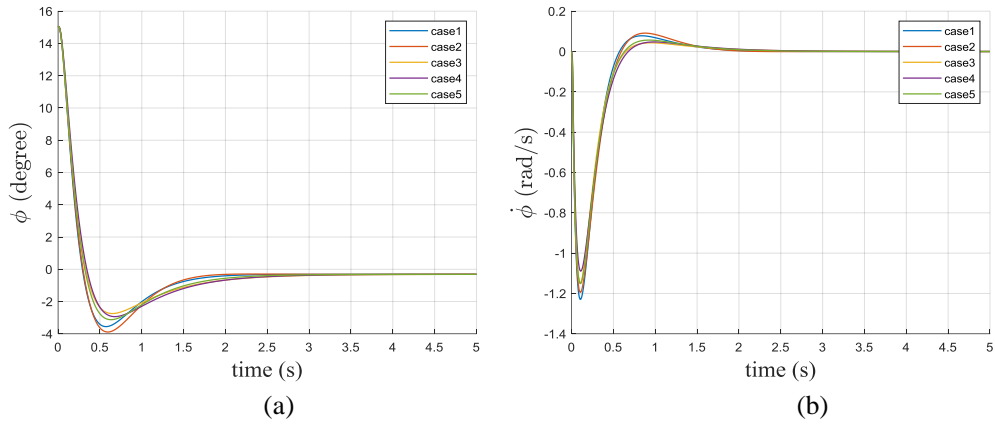
Figure 4.8. Response of: (a) roll displacement (b) roll rate
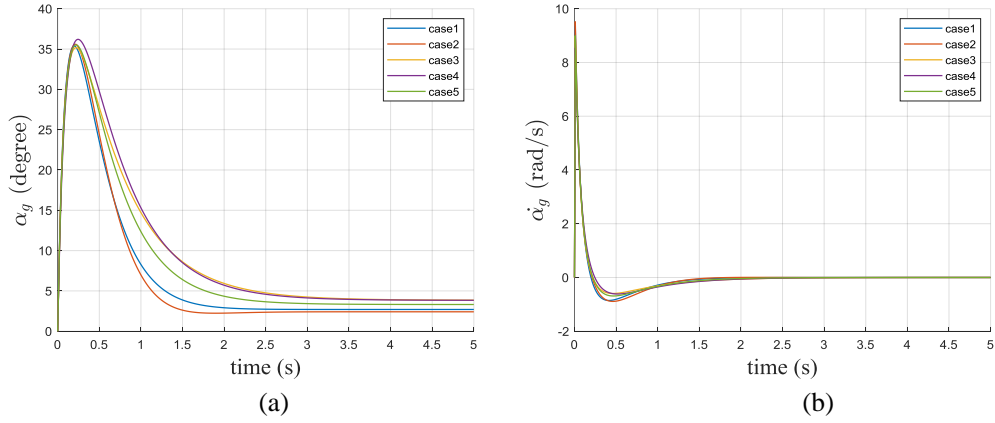
Figure 4.9. Response of: (a) shaft displacement (b) shaft rate

After tuning weighting factors, we noted that all tuning cases can correspond with the specified design goals given in the introduction. An adjustment of the weighting factors to get a controller more in line with the specified design goals must be performed. However, difficulty in finding the right weight factors limits the application of the LQR based controller synthesis. By tuning, the state weighting matrix is selected in case 2.

However, the steady state error is not zero for both vehicle and shaft motor. In this particular project we want to stabilize the vehicle around its vertical orientation. That means we try to force the roll angle ϕ to track the zero-reference signal. Moreover, we should keep the precession angles as close to zero as possible.

Based on the selected weighting matrices, the optimal gain of LQR is obtain as follows

$$K = \begin{bmatrix} 77.3451 & 10 & 10.3127 & -0.5371 & -1.0885 \end{bmatrix} \qquad (4.2.5)$$

4.2.3   Disturbance rejection test

Depending on what one considers more important, one can choose any setting weights from the Table 3.1. At this point, we will check the robustness of the 2nd case. In order to evaluate the robustness of the controllers, the obtained state-feedback controller then applied with an impulse disturbance. Figure 4.10 shows the performance of the vehicle angle and vehicle angular velocity to an initial position and an impulse disturbance at 5s. from an initial angle $18°$, the vehicle takes take 2s to return to the equilibrium, moreover it takes to 2s to reject the disturbance. The performance of the shaft motor angle and shaft motor angular velocity are demonstrated in Figure 4.11. We try to increase lean angle of vehicle, but we also prevent the shaft motor not bigger than the boundaries of range $\pm45°$.

Our simulation succeeds to confront the disturbances and it gets stabilized in its upright position. Consequently, we can claim that the system successfully rejects disturbances.
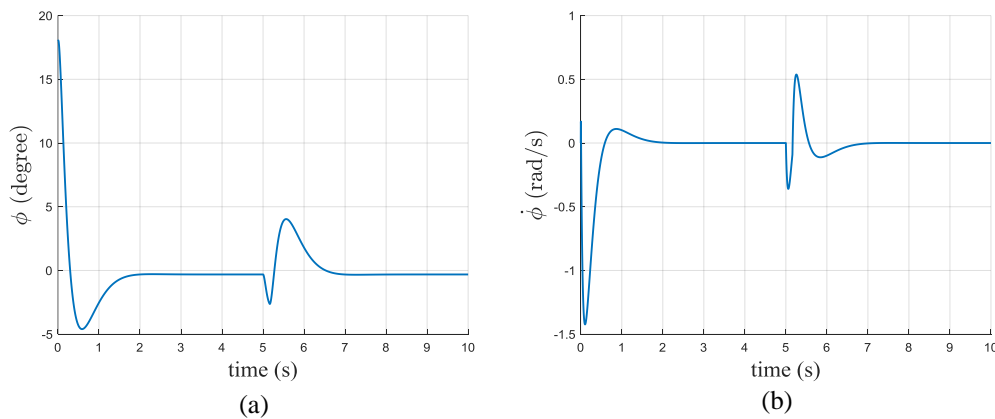
Figure 4.10. Response of (a) vehicle angle and (b) vehicle angular velocity to an initial position and impulse disturbance

51
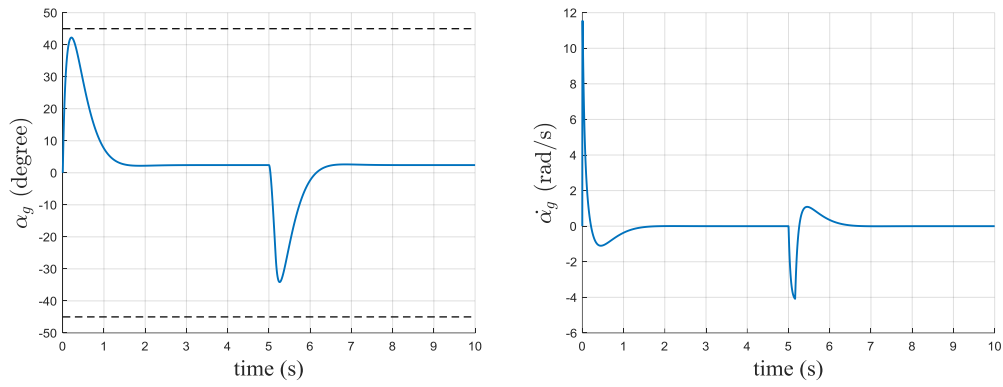
Figure 4.11. Response of (a) shaft angle and (b) shaft angular velocity to an initial position and impulse disturbance

This page is blank

CHAPTER 5

CONCLUSION

Two control strategies are developed to stabilize two-wheeled vehicle. Numerical simulations are used to illustrate the performance of the controller. In this section we review our research and suggest future work.

5.1   Summary

In this thesis presents the gyroscopic stabilization for the two-wheeled vehicle. The nonlinear equations of motion are developed to express the concept vehicle using Lagrangian mechanics. To simplify the equation of motion, we linearize the dynamics about an equilibrium at its upright position. Later, we marge together equation of transmission system that drive each gimbal and the model of DC motor. After analysing the stability and the controllable of the open loop system, the system was verified. Then we purpose two controllers; a cascade PID controller, and an LQR controller. For each controller, we initialized our vehicle from a tilted position that never exceeded the range $\pm 15°$, to avoid the shaft motor reaching close to the boundaries of range $\pm 45°$.

After the vehicle turns to the equilibrium point, the cascade PID controller not only cannot maintain the shaft motor to zero position, then the shaft motor remains slowly moving. In most cases, not only we require to stabilize the vehicle on its upright position, but we also want to keep the gyroscopes to the zero position as much as possible, so they can offset disturbances that might happen. On the other hand, if the gimbal angle were not returned to zero after stabilizing the vehicle then the gyro would not be proficient of producing its maximum reaction torque for the next disturbance introduced into the system which could feasibly not be enough to stabilize the vehicle. In the comparison of six setting controls, the vehicle takes the shortest time about 0.85s to return to the equilibrium position when the setting is given in case 6.

With the LQR controller, we achieved good response. In this particular project our task is to stabilize the static vehicle starting from some initial roll-angle. We have already proved the necessity of driving the precession angles of the

gyroscopes close to zero. Linear model is used to check performance of the performance of the weighting matrix. For the nonlinear model, the vehicle and the shaft motor take shortest time about 2 s to return to the equilibrium position when the weighting is given in case 2, but the shaft motor's angular velocity is about 16 rad/s. For the disturbance rejection test, the simulation succeeds to handle the disturbances and it secures stabilized in its upright position. As a result, the system can be ensured that it successfully rejects disturbances.

5.2 Recommended Future Work

The focus of this research was to model the two-wheeled vehicle by compare two feedback controllers: the cascade PID controller and the LQR controller. There are many areas that would be interesting to continue exploring with this system. Suggestions from gyroscopic two-wheeled vehicle system research are as follows:

1. Having met all the above specifications, the next step is to study and investigate gyro-based stabilizing controllers with prototype. The prototype of the gyroscopic two-wheeled vehicle is already produced and installed. Synthesis these controllers to test and check the response for the actual experiment.

2. In this thesis we only studied the control dynamics of the static vehicle. This is actually the most challenging feature of the active gyroscopic roll-stabilizer with the trajectory tracking. After obtaining the proper controller for the static case (regulator problem), the next step is to investigate the full dynamics of the vehicle and track a trajectory. The faster the speed of the vehicle is, the less balancing torque will be required from the gyroscopes.

3. In this project we have focused on the transportation perspective. However, there are several applications waiting for the gyro-stabilizers to implement. Self-balancing robots can also use gyro-stabilizers to maintain a reference orientation.

This page is blank

REFERENCES

[1]   T. Náhlík and D. Smetanová, "Applications of Gyroscopic Effect in Transportation," *NAŠE MORE Znan. časopis za more i Pomor.*, vol. 65, no. 4 Special issue, pp. 293–296, 2018.

[2]   L. Brennan, "Means for imparting stability to unstable bodies." Google Patents, Aug. 08, 1905.

[3]   P. Schilowsky, "Gyroscope." Google Patents, Apr. 27, 1915.

[4]   M. P. Schilowsky, "Demonstration of Some Applications of the Gyroscope," *Proc. Phys. Soc. London*, vol. 35, no. 1, p. 125, 1922.

[5]   P. Schilowsky, "Monotrack-vehicle." Google Patents, Oct. 15, 1912.

[6]   T.-K. Dao and C.-K. Chen, "Sliding-mode control for the roll-angle tracking of an unmanned bicycle," *Veh. Syst. Dyn.*, vol. 49, no. 6, pp. 915–930, 2011.

[7]   T.-K. Dao and C.-K. Chen, "Path tracking control of a motorcycle based on system identification," *IEEE Trans. Veh. Technol.*, vol. 60, no. 7, pp. 2927–2935, 2011.

[8]   Y. Tanaka and T. Murakami, "Self sustaining bicycle robot with steering controller," in *The 8th IEEE International Workshop on Advanced Motion Control, 2004. AMC'04.*, 2004, pp. 193–197.

[9]   L. Keo and Y. Masaki, "Trajectory control for an autonomous bicycle with balancer," in *2008 IEEE/ASME International Conference on Advanced Intelligent Mechatronics*, 2008, pp. 676–681.

[10]   M. Yamakita, A. Utano, and K. Sekiguchi, "Experimental study of automatic control of bicycle with balancer," in *2006 IEEE/RSJ International Conference on Intelligent Robots and Systems*, 2006, pp. 5606–5611.

[11]   T.-D. Chu and C.-K. Chen, "Design and implementation of model predictive control for a gyroscopic inverted pendulum," *Appl. Sci.*, vol. 7, no. 12, p. 1272, 2017.

[12] S. C. Spry and A. R. Girard, "Gyroscopic stabilisation of unstable vehicles: configurations, dynamics, and control," *Veh. Syst. Dyn.*, vol. 46, no. S1, pp. 247–260, 2008.

[13] P. Y. Lam, "Gyroscopic stabilization of a kid-size bicycle," in *2011 IEEE 5th International Conference on Cybernetics and Intelligent Systems (CIS)*, 2011, pp. 247–252.

[14] D. K. Y. Kim and K. Bretney, "Electrical system for gyroscopic stabilized vehicle." Google Patents, Dec. 23, 2014.

[15] M.-H. Hsieh, Y.-T. Chen, C.-H. Chi, and J.-J. Chou, "Fuzzy sliding mode control of a riderless bicycle with a gyroscopic balancer," in *2014 IEEE International Symposium on Robotic and Sensors Environments (ROSE) Proceedings*, 2014, pp. 13–18.

[16] B. R. Holstein, "Gyroscope precession and general relativity," *Am. J. Phys.*, vol. 69, no. 12, pp. 1248–1256, 2001.

[17] A. Iggidr, "Controllability, Observability, and Stability of Mathematical Models." 2004.

[18] J. Klamka, "System Characteristics: Stability, Controllability, Observability," *Control Syst. Robot. Autom.*, vol. 7, pp. 232–247, 2009.

[19] C. Hajiyev, H. E. Soken, and S. Y. Vural, "Linear Quadratic Regulator Controller Design," in *State Estimation and Control for Low-cost Unmanned Aerial Vehicles*, Springer, 2015, pp. 171–200.

[20] A. B. C. E.-V. N. Katsikis, "PID Control Design," Rijeka: IntechOpen, 2012, p. Ch. 1.

[21] R. Eide, P. M. Egelid, and H. R. Karimi, "LQG control design for balancing an inverted pendulum mobile robot," *Intell. Control Autom.*, vol. 2, no. 02, p. 160, 2011.

[22] S. Trimpe, A. Millane, S. Doessegger, and R. D'Andrea, "A self-tuning LQR approach demonstrated on an inverted pendulum," *IFAC Proc. Vol.*, vol. 47,

no. 3, pp. 11281–11287, 2014.

This page is blank

APPENDIX
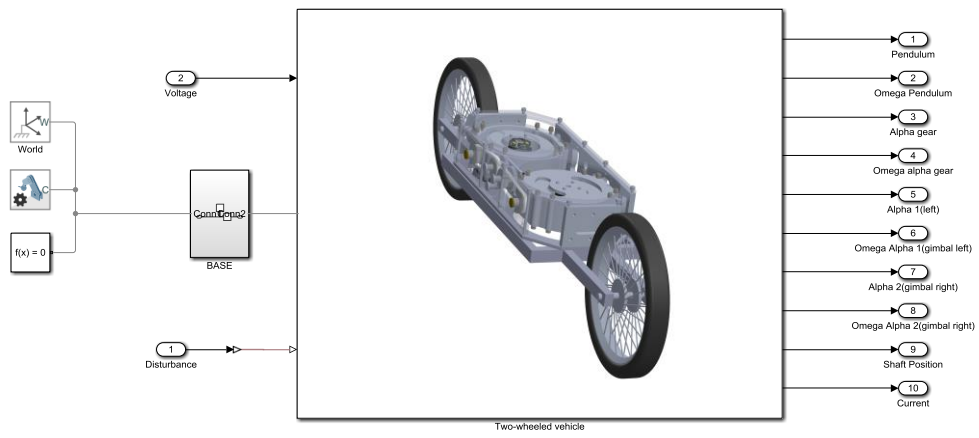
Figure 5.1. Model simulink two-wheeled vehicle
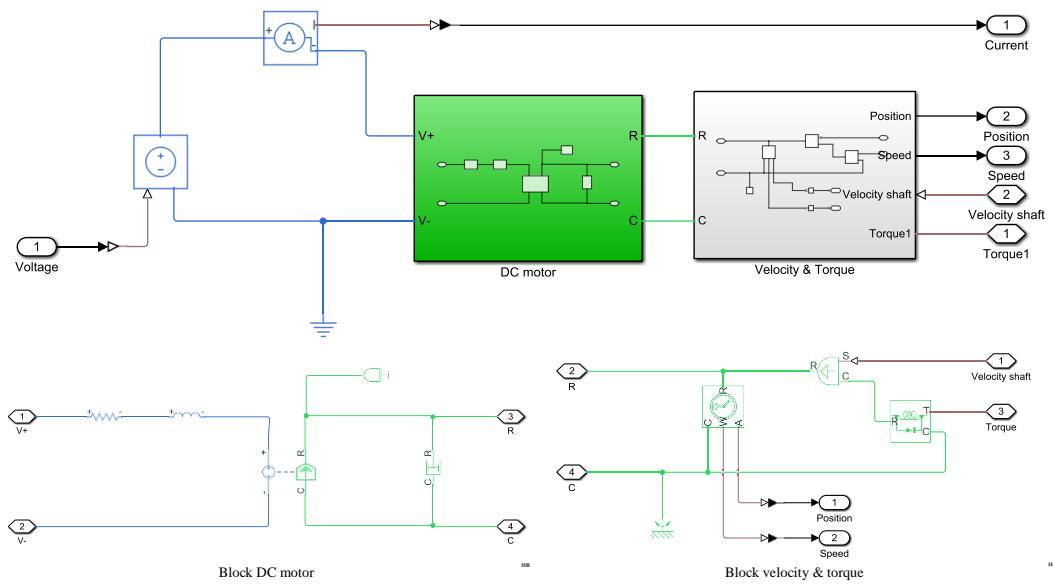
Figure 5.2. Model simulink DC motor

Figure 5.3. Assembly part in Simcape Multibody